BAMS Article

Advances in the Subseasonal Prediction of Extreme Events

Relevant Case Studies across the Globe

Daniela I. V. Domeisen, Christopher J. White, Hilla Afargan-Gerstman, Ángel G. Muñoz, Matthew A. Janiga, Frédéric Vitart, C. Ole Wulff, Salomé Antoine, Constantin Ardilouze, Lauriane Batté, Hannah C. Bloomfield, David J. Brayshaw, Suzana J. Camargo, Andrew Charlton-Pérez, Dan Collins, Tim Cowan, Maria del Mar Chaves, Laura Ferranti, Rosario Gómez, Paula L. M. González, Carmen González Romero, Johnna M. Infanti, Stelios Karozis, Hera Kim, Erik W. Kolstad, Emerson LaJoie, Llorenç Lledó, Linus Magnusson, Piero Malguzzi, Andrea Manrique-Suñén, Daniele Mastrangelo, Stefano Materia, Hanoi Medina, Lluís Palma, Luis E. Pineda, Athanasios Sfetsos, Seok-Woo Son, Albert Soret, Sarah Strazzo, and Di Tian

ABSTRACT: Extreme weather events have devastating impacts on human health, economic activities, ecosystems, and infrastructure. It is therefore crucial to anticipate extremes and their impacts to allow for preparedness and emergency measures. There is indeed potential for probabilistic subseasonal prediction on time scales of several weeks for many extreme events. Here we provide an overview of subseasonal predictability for case studies of some of the most prominent extreme events across the globe using the ECMWF S2S prediction system: heatwaves, cold spells, heavy precipitation events, and tropical and extratropical cyclones. The considered heatwaves exhibit predictability on time scales of 3–4 weeks, while this time scale is 2–3 weeks for cold spells. Precipitation extremes are the least predictable among the considered case studies. Tropical cyclones, on the other hand, can exhibit probabilistic predictability on time scales of up to 3 weeks, which in the presented cases was aided by remote precursors such as the Madden–Julian oscillation. For extratropical cyclones, lead times are found to be shorter. These case studies clearly illustrate the potential for event-dependent advance warnings for a wide range of extreme events. The subseasonal predictability of extreme events demonstrated here allows for an extension of warning horizons, provides advance information to impact modelers, and informs communities and stakeholders affected by the impacts of extreme weather events.

KEYWORDS: Madden-Julian oscillation; Severe storms; Ensembles; Forecast verification/skill; Probability forecasts/models/distribution; Flood events

https://doi.org/10.1175/BAMS-D-20-0221.1

Corresponding author: Daniela I. V. Domeisen, daniela.domeisen@env.ethz.ch

In final form 16 February 2022

AFFILIATIONS: Domeisen—University of Lausanne, Lausanne, and ETH Zurich, Zurich, Switzerland; **White**—Department of Civil and Environmental Engineering, University of Strathclyde, Glasgow, United Kingdom; **Afargan-Gerstman**—Institute for Atmospheric and Climate Science, ETH Zurich, Zurich, Switzerland; **Muñoz and González Romero**—International Research Institute for Climate and Society, Columbia Climate School, and The Earth Institute, Columbia University, New York, New York; **Janiga**—Naval Research Laboratory, Monterey, California; **Vitart, Ferranti, and Magnusson**—European Centre for Medium-Range Weather Forecasts, Reading, United Kingdom; **Wulff**—Institute for Atmospheric and Climate Science, ETH Zurich, Zurich, Switzerland, and Norwegian Research Centre, Bjerknes Centre for Climate Research, Bergen, Norway; **Antoine, Ardilouze, and Batté**—CNRM, Université de Toulouse, Météo-France, CNRS, Toulouse, France; **Bloomfield**—Department of Meteorology, University of Reading, Reading, and School of Geographical Sciences, University of Bristol, Bristol, United Kingdom; **Brayshaw and Charlton-Pérez**—Department of Meteorology, University of Reading, Reading, United Kingdom; **Camargo**—Lamont-Doherty Earth Observatory, Columbia University, Palisades, New York; **Collins, Infanti, and LaJoie**—Climate Prediction Center, NOAA/NWS/NCEP, College Park, Maryland; **Cowan**—Centre for Applied Climate Sciences, University of Southern Queensland, Toowoomba, Queensland, and Bureau of Meteorology, Melbourne, Victoria, Australia; **del Mar Chaves* and Materia**—Climate Simulations and Predictions, Centro Euro-Mediterraneo sui Cambiamenti Climatici, Bologna, Italy; **Gómez**—Organismo Internacional Regional de Sanidad Agropecuaria, San Salvador, El Salvador; **González**—National Centre for Atmospheric Science, Department of Meteorology, University of Reading, United Kingdom, and International Research Institute for Climate and Society, The Earth Institute, Columbia University, New York, New York; **Karozis and Sfetsos**—National Centre for Scientific Research "Demokritos," Athens, Greece; **Kim and Son**—School of Earth and Environmental Sciences, Seoul National University, Seoul, South Korea; **Kolstad**—Norwegian Research Centre, Bjerknes Centre for Climate Research, Bergen, Norway; **Lledó, Manrique-Suñén, Palma, and Soret**—Barcelona Supercomputing Center, Barcelona, Spain; **Malguzzi and Mastrangelo**—CNR-ISAC, Bologna, Italy; **Medina and Tian**—Department of Crop, Soil, and Environmental Sciences, Auburn University, Auburn, Alabama; **Pineda**—School of Earth Sciences, Energy and Environment, Yachay Tech University, Urcuquí, Ecuador; **Strazzo**—Embry–Riddle Aeronautical University, Daytona Beach, Florida
***Current affiliation:** University of Bologna, Bologna, Italy

Extreme weather events pose threats to humans, infrastructure, and ecosystems. In a changing climate, many extremes are projected to increase in strength, frequency, and/or duration, and it is therefore increasingly important to anticipate extreme events and their impacts as early as possible. A successful prediction several weeks in advance will benefit stakeholders' decision-making for emergency management (White et al. 2017; Merz et al. 2020; White et al. 2022). Indeed, there is increasing potential for probabilistic subseasonal prediction on time scales of several weeks for extreme events (Vitart 2014; Vitart and Robertson 2018; Robertson et al. 2020). Increased predictability can arise from remote drivers or long-lived precursor patterns that are conducive to the occurrence of extreme events. These drivers include tropical precursors such as the Madden–Julian oscillation (MJO) (e.g., Vitart and Molteni 2010; Rodney et al. 2013) and El Niño–Southern Oscillation (ENSO) (e.g., Domeisen et al. 2015), surface interactions with snow cover (e.g., Cohen and Jones 2011) or sea ice (e.g., Sun et al. 2015), the upper atmosphere (e.g., Domeisen et al. 2020b; Domeisen and Butler 2020), or a combination of predictors (Muñoz et al. 2015, 2016; Doss-Gollin et al. 2018; Dobrynin et al. 2018). A better understanding of these precursors can contribute

to increased predictability. At the same time, improvements in the prediction of extremes arise from progress in the performance of prediction systems through advancements in process representation, coupling, and parameterization, as well as model resolution (Bauer et al. 2015). Merryfield et al. (2020) recommended an assessment of the predictability of historical high-impact weather events as a way forward to demonstrate the potential benefits of subseasonal-to-seasonal (S2S) forecasts. Here we discuss extreme event predictability based on a state-of-the-art subseasonal prediction system and a range of precursors for selected case studies of high-impact extremes in Europe, Africa, Asia, and Australia, as well as South, Central, and North America for the most prominent types of extreme events on a global scale: heatwaves, cold spells, heavy precipitation events, and both tropical and extratropical cyclones. The following sections provide a brief overview of the physical drivers and potential for predictability for these extreme events, while the subsequent sections dive into the specific case studies.

Heatwaves. Heatwaves over land have devastating impacts on human health and ecosystems (Campbell et al. 2018; Yang et al. 2019), agriculture (Brás et al. 2021), and energy demand (Auffhammer et al. 2017; Bloomfield et al. 2020). Over the past decades, heatwaves have significantly increased in frequency and intensity (Perkins et al. 2012) with further increases predicted for the future (Watanabe et al. 2013; Lopez et al. 2018), largely due to anthropogenic global warming (IPCC 2013; Shiogama et al. 2014). Heatwaves are commonly characterized by temperature and duration thresholds (Russo et al. 2014), in addition to humidity and diurnal temperature cycle characteristics for applications to human morbidity and mortality (e.g., Raymond et al. 2020).

Heatwaves are often associated with persistent anticyclonic circulation patterns (Li et al. 2015; Freychet et al. 2017) that can sometimes be identified as blocking (Pfahl and Wernli 2012; Schaller et al. 2018; Brunner et al. 2018; Carrera et al. 2004; Dong et al. 2018; Li et al. 2019; Yeo et al. 2019), long-lived Rossby wave packets (RWPs; Wirth et al. 2018), which can contribute to predictability (Fragkoulidis et al. 2018; Grazzini and Vitart 2015), or quasi-stationary wave trains (Enomoto 2004; Kim et al. 2018; Li et al. 2019). These patterns can be triggered or enhanced by remote effects. For instance, sea surface temperature (SST) anomalies in subtropical and extratropical ocean basins can help induce European and North American heatwaves (Wulff et al. 2017; Duchez et al. 2016; McKinnon et al. 2016; Hartmann 2015), and East Asian heatwaves can be triggered by the North Atlantic Oscillation (NAO), Ural blocking, and diabatic heating in the eastern Mediterranean (Yasui and Watanabe 2010; Sun 2012; Wu et al. 2016; Gao et al. 2018; Li et al. 2019).

These remote forcings can enhance the predictability of heatwaves. Recent research has indeed shown potential for the extended-range prediction of heatwaves on subseasonal-to-seasonal time scales (Kueh and Lin 2020; Koster et al. 2010; Luo and Zhang 2012; Pepler et al. 2015; Tian et al. 2017; Wulff and Domeisen 2019). In addition, heatwaves can also be exacerbated by land–atmosphere feedbacks (e.g., Fischer et al. 2007; Mueller and Seneviratne 2012; Miralles et al. 2014; Hauser et al. 2016; Seneviratne et al. 2010; Berg and Sheffield 2018; Tian et al. 2016, 2018) and improvements in soil moisture initialization can therefore increase the predictability of heatwaves (Ferranti and Viterbo 2006; Dirmeyer et al. 2018; Bunzel et al. 2018).

Cold spells. Cold spells can affect electricity production (Beerli et al. 2017; Gruber et al. 2021; Doss-Gollin et al. 2021) and demand (Cradden and McDermott 2018; Bloomfield et al. 2018, 2020), human mortality (Charlton-Perez et al. 2019, 2021), and agriculture (Materia et al. 2020). Similar to heatwaves, cold spells are often defined by temperature and duration thresholds (de Vries et al. 2012). Like heatwaves, cold spells can be related to atmospheric

blocking, and hence, model biases in blocking frequency can impair predictions at lead times beyond 2 weeks (Hamill and Kiladis 2014; Quinting and Vitart 2019). Predictability can be gained from tropical drivers such as the MJO, and model performance can be enhanced by capturing the predictable signal of large-scale weather patterns such as the NAO at the extended range (Ferranti et al. 2018). Blocking associated with the negative phase of the NAO can also be induced through sudden stratospheric warming (SSW) events (Thompson et al. 2002; Lehtonen and Karpechko 2016; Charlton-Perez et al. 2018; Domeisen 2019), which can induce cold spells over both land (Kolstad et al. 2010) and ocean (Afargan-Gerstman et al. 2020). However, not all regions gain predictability skill from stratospheric forcing (Domeisen et al. 2020b; Materia et al. 2020).

Precipitation events. Heavy precipitation events can lead to flooding as well as land- or mudslides, and they are often accompanied by strong winds and low temperatures, the combination of which can be detrimental to humans, agriculture, and infrastructure (Zscheischler et al. 2020). Heavy precipitation events are projected to become more frequent in many regions (Donat et al. 2016; Prein et al. 2017) due to anthropogenic climate change (Westra et al. 2013; Zhang et al. 2013; C. Li et al. 2021). Similar to temperature extremes, rainfall extremes arise through persistent atmospheric conditions, which can be triggered or maintained by large-scale forcing, e.g., from ENSO and the MJO (Jones et al. 2004; Kenyon and Hegerl 2010; Muñoz et al. 2015), atmospheric blocking (Lenggenhager and Martius 2019), or monsoon systems (Zhang and Zhou 2019).

Precipitation extremes tend to be less predictable than temperature extremes such as warm and cold spells (de Andrade et al. 2019). The ability of a prediction system to predict rainfall extremes beyond deterministic time scales is related to the simulation of the connection between precipitation and its large-scale forcing such as ENSO and the MJO (Vigaud et al. 2017; Specq et al. 2020) or atmospheric rivers (DeFlorio et al. 2019). Regions with strong ENSO teleconnections exhibit better predictability of rainfall extremes, as, for example, in Australia (King et al. 2020) or the southwestern United States (Gershunov 1998; Pan et al. 2019), if ENSO is correctly simulated (Bayr et al. 2019). Interference of drivers on multiple time scales can further modulate the intensity, occurrence, and predictability of precipitation extremes (Muñoz et al. 2015, 2016).

Tropical cyclones and medicanes. Tropical and extratropical cyclones impact human lives and livelihoods and lead to large environmental impacts and economic losses (Camargo and Hsiang 2015; Hsiang 2010; Hsiang and Narita 2012). Anthropogenic climate change affects various properties of tropical cyclones (TC), in particular their intensity, as well as the precipitation and storm surge associated with these events (Knutson et al. 2019, 2020). While individual cyclones' genesis, tracks and intensity are not predictable beyond deterministic time scales, large-scale drivers can provide predictability in a probabilistic sense on S2S time scales. On seasonal time scales, ENSO modifies the characteristics of TC frequency, intensity, and tracks (e.g., Vitart et al. 2003; Lin et al. 2017; Nicholls 1979; Evans and Allan 1992). On subseasonal time scales, TC activity is enhanced (decreased) during and after an active (suppressed) MJO (e.g., Camargo et al. 2019), especially in the Southern Hemisphere (e.g., Hall et al. 2001; Camargo et al. 2009), allowing for successful statistical forecasts (Leroy and Wheeler 2008). Recently, the performance of dynamical models for forecasting TCs on subseasonal time scales has significantly improved (Camp et al. 2018; Camargo et al. 2019; Robertson et al. 2020; Vitart et al. 2010; Camargo et al. 2021). A successful example is Cyclone Hilda, which made landfall in northwestern Australia and was predicted 3 weeks in advance (Gregory et al. 2019). However, this success is not consistent across models, and is likely linked to a successful prediction of the MJO (Vitart 2017; Lee et al. 2018, 2020).

In addition to tropical cyclones, we also consider *medicanes* ("Mediterranean hurricanes"), rare intense and high-impact extratropical cyclones in the Mediterranean region (Ulbrich et al. 2009; Cavicchia et al. 2014; Mylonas et al. 2018; Flaounas et al. 2021). These events occur on average 1.6 times per year (Flaounas et al. 2015) and can lead to severe damage in coastal areas associated with flooding and high winds.

Data and methods

To evaluate the subseasonal prediction of the above extreme events we use both forecasts and hindcasts (historical forecasts) from the extended-range operational ensemble prediction system (Vitart et al. 2008) from the European Centre for Medium-Range Weather Forecasts (ECMWF), which is part of the S2S database (Vitart et al. 2017). The prediction system includes coupling with the ocean and sea ice (Buizza et al. 2017). The atmospheric model has a horizontal resolution of approximately 36 km and 91 vertical levels with a model lid at 0.01 hPa (at the time of data download for this study). Where available, that is, for case studies after June 2015, forecasts from the prevailing model version were used (cycles 43R1, 43R3, and 45R1); these ensemble forecasts consist of 51 members. For the case studies using hindcasts, the 11-member hindcast ensemble from model cycle 46R1 was used. Both forecasts and hindcasts are initialized twice weekly.

The target weeks are selected for each case study individually based on the week of the most extreme anomalies. Since the forecasts are only initialized twice weekly, it is not always possible to find a forecast that is initialized exactly the day before week 1. Week-1 lead time for a specific case study is therefore chosen such that the target week lies directly on or after the initialization, that is, the forecast is initialized either on the first day of week 1 or up to 2 days earlier. The additional forecast lead weeks (weeks 2–4) then lie exactly adjacent to week 1.

To compute anomalies for the subseasonal predictions, a 7-day mean climatology is computed based on the 11-member ensemble hindcasts initialized for the same lead time for the corresponding available 20-yr hindcast period. For example, for the California heatwave on 23 July 2018, the corresponding week-1 climatology is based on the ensemble mean of the hindcast ensemble initialized on 23 July for each year from 1998 to 2017. The climatology is computed for each lead week separately, yielding a lead-time dependent climatology. Anomalies for the predictions are then computed by subtracting the model climatology from each ensemble member. For the earlier case studies, the climatology is computed over a 19-yr hindcast period excluding the year of the case study to simulate an operational prediction setting. Anomalies for reanalysis are computed in a consistent way, by subtracting the daily mean climatology computed from reanalysis data for the same years that are used for computing the hindcast climatology for each case study. The use of anomalies for the model and reanalysis with respect to their respective climatologies provides a simple bias correction.

The temperature predictions are verified against the 2-m temperatures from ERA5 (Hersbach et al. 2020), as temperatures are well represented in reanalysis. Precipitation can show greater biases in reanalysis (Alexander et al. 2020); hence, precipitation is verified against observational datasets from the Australian Water Availability Project (AWAP) 5-km daily gridded rainfall analysis (Jones et al. 2009) and the CPC Global Unified Gauge-Based Analysis of Daily Precipitation (Chen et al. 2008).

The temperature extremes case studies compare the probability density functions (PDFs) of the ensemble members for different lead weeks. Tercile limits (below normal, normal, and above normal, as well as the 10th and the 90th percentiles) are computed with respect to the lead time–dependent model climatology, based on 11 hindcast members. For the rainfall extremes, forecast performance is assessed by measuring the forecast system's association and discrimination attributes, using the Spearman correlation coefficient (Wilks 2019) and

the area under the relative operating characteristic (ROC; Wilks 2019) curve for the above-normal category, respectively. The Spearman correlation is a nonparametric measure of how in-phase the forecasts and observations are (correlation values of 1 indicate perfect association), and the ROC area for the above-normal category measures how well the forecast system discriminates between the above-normal and the other tercile-based categories, with values at 50% indicating a discrimination as good as that of climatology-based forecasts, and values above (below) 50% indicating better (worse) discrimination than climatology-based forecasts. The precipitation forecasts are calibrated according to a pattern-based model output statistics approach using canonical correlation analysis (CCA; Tippett et al. 2008), implemented via PyCPT, a set of Python libraries interfacing the Climate Predictability Tool (Muñoz 2020; Muñoz et al. 2019; Mason et al. 2021), using IRI's "NextGen" forecast approach (Muñoz et al. 2019; WMO 2020). To obtain a robust sample size, these metrics were computed using all eight initializations (20 years per initialization) available for the months and target dates listed in Table 1, conducted independently for each rainfall extreme case study. For example, for the Guatemala case study (see next section), eight 20-yr-long hindcasts were used, corresponding to all initializations available for June 1998–2017, providing a total of 160 hindcast weeks to compare against the corresponding 160 weeks of observed rainfall. For additional details, see Materia et al. (2020).

For evaluating the model performance for the cyclones, their observed tracks are compared against the probability of cyclone occurrence given by the probability of a cyclone passing within 300 km of each grid point using the ECMWF tracker (Vitart et al. 1997) from the 51-member ensemble of the prediction system. The observed tropical cyclones data are obtained from the International Best Track Archive for Climate Stewardship (IBTrACS) (Knapp et al. 2010). The observed track for the medicane is obtained from the ECMWF operational analysis. The medicane is further evaluated using convective available potential energy

Table 1. Overview of the case studies evaluated in this study.

Location/target region	Forecast target period
Heatwaves	
Western United States (California) (32°–48°N, 110°–125°W)	23–29 Jul 2018
Central/northeastern Europe (50°–60°N, 10°–20°E)	23–29 Jul 2018
Southeastern United States (25°–45°N, 92°–70°W)	24–30 May 2019
East Asia (eastern China, Korean Peninsula, Japan) (30°–40.5°N, 105°–130.5°E)	5–11 Aug 2013
Cold spells	
Southeastern Europe (37.5°–54°N, 10.5°–30°E)	3–9 Apr 2003
Central/northern Europe (37.5°–65°N, 12.5°W–30°E)	26 Feb–3 Mar 2018
Southwestern Europe (France) (43.5°–49.5°N, 4.5°W–7.5°E)	16–22 Jan 2017
Northern Europe (United Kingdom, Germany, Scandinavia) (45°–65°N, 10°W–30°E)	27 Nov–3 Dec 2010
Precipitation events	
Volcán de Fuego, Guatemala (14.5°N, 91°W)	18–24 Jun 2018
Northwestern Ecuador (0°, 79°W)	21–27 Jan 2016
Northwestern Italy (43.5°–46.5°N, 6.5°–10°E)	21–27 Nov 2016
Northeastern Australia (18°–22°S, 138°–147°E)	31 Jan–6 Feb 2019
Cyclones	
Western Australia: Cyclone Claudia (no landfall)	5 Jan 2020 (formation)/18 Jan 2020 (dissipation)
Mozambique Channel: Cyclone Belna (landfall: Madagascar)	2 Dec 2019 (formation)/9 Dec 2019 (landfall)
Western North Pacific: Typhoon Chan-hom (landfall: China)	29 Jun 2015 (formation)/11 Jul 2015 (landfall)
Mediterranean: Medicane Zorbas (landfall: Peloponnese, Greece)	27 Sep 2018 (formation)/29 Sep 2018 (landfall)

(CAPE), an indicator of atmospheric instability, which is a necessary condition for the development of severe weather events. CAPE has been found to be a prominent indicator and potential predictor for tropical cyclones (Huang and Liang 2010; Lee and Frisius 2018; Mylonas et al. 2018) but has not been prominently used for medicanes.

Extreme event case studies

This section presents specific case studies for the four types of extremes. The case studies were selected based on their extreme nature and societal impacts. While this selection should not be seen as a complete assessment of model performance or intercomparison of predictability between event types or within the same event type, these case studies serve as a representative selection of extreme events and their predictability, which can translate into time scales of emergency preparedness (White et al. 2022). Table 1 provides an overview of the timing and location of each case study.

Heatwaves. We first examine the predictability of four extreme heatwaves in North America, Europe, and East Asia between 2013 and 2019 (Fig. 1). The first two heatwaves are part of the extreme Northern Hemisphere heatwave in summer 2018, when heatwaves simultaneously affected North America and Eurasia. We focus on the week of 23–29 July 2018, when temperatures over California reached 51°C in Death Valley. California monthly mean temperatures for July surpassed the previous record set in 1931 (NOAA 2018) as heatwaves also occurred earlier that month. Similarly in Europe, the seasonal mean was strongly affected as the heat arrived in two waves, one from mid-May to mid-June and the second from mid-July to the beginning of August.

The model successfully predicts the concurrent 2018 heatwaves for the target period 3 weeks ahead in terms of the spatial structure of the anomalies for both considered regions, although with reduced amplitudes, meaning that most ensemble members remain well below the observed anomalies (Figs. 1a–d). For Europe, at lead times of 2 weeks, 49 out of 50 ensemble members exceed the upper third of the climatological distribution (Fig. 2b). The forecast probability for the upper tercile is still 86% at lead times of 3 weeks and reduces to 60% for lead week 4, but with a long tail of the distribution toward extreme heat. For California, the model also predicts the extreme heat with some confidence out to 4 weeks (Fig. 2a). The 2-week lead forecast yields the most confident prediction, with 29% of ensemble members predicting temperatures above the 90th percentile, and 78% predicting above-normal temperatures. Interestingly, although the 3-week lead forecast distribution is still shifted toward above-normal temperatures, it is arguably the weakest prediction, with only 12% of members predicting temperatures above the 90th percentile, as compared to 24% for week 4.

Generally, California/western U.S. heatwaves tend to be associated with high pressure over the Great Plains, low pressure off the California coast, and warm moist air transport from the south. There has been an increasing trend in this type of humid heatwave in recent years due to warming ocean temperatures (Gershunov and Guirguis 2015). When present, this ocean–atmosphere pattern can lead to higher predictability of heatwaves, although forecast accuracy over the western United States and California is on average lower relative to other U.S. regions (Gershunov and Guirguis 2012; Ford et al. 2018; Kornhuber et al. 2019). However, July 2018 was atypical in that it was characterized by a wave-7 pattern (Kornhuber et al. 2019) associated with a strong and persistent region of high temperatures over much of the United States in the first half of July, and high pressure anomalies off the coast of and over the western United States in the last 2 weeks of July. Land–atmosphere and vegetation feedbacks are further suggested to have played a role in the 2018 heatwave, especially over central Europe (Liu et al. 2020; Sinclair et al. 2019; Albergel et al. 2019). Finally, the event was made more likely due to anthropogenic climate change (Yiou et al. 2019).

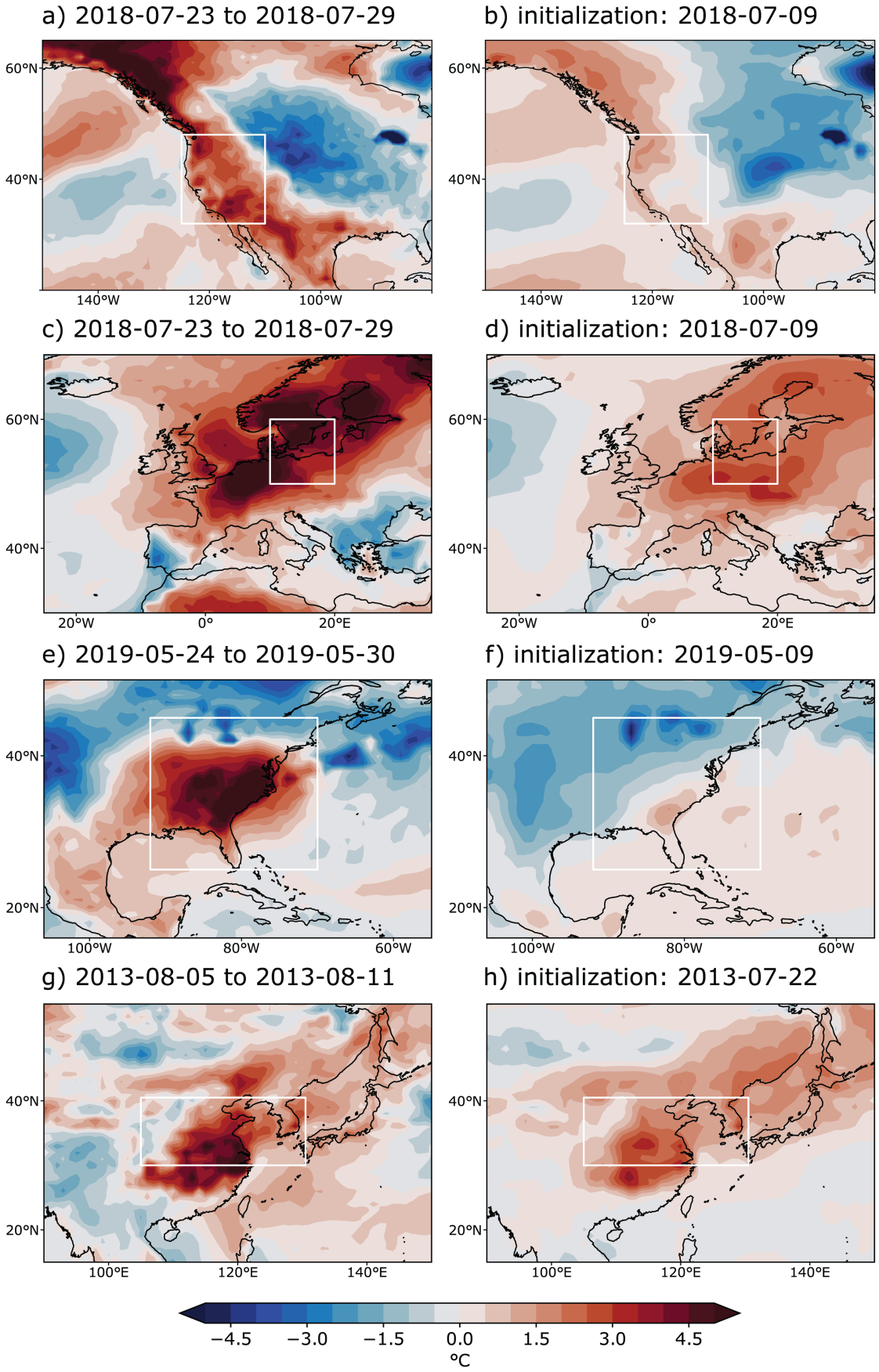

Fig. 1. Heatwaves: (a),(c),(e),(g) 2-m temperature anomalies for the target week (indicated in the panel titles) from ERA5 data and (b),(d),(f),(h) those predicted by the ECMWF week-3 forecasts (hindcasts prior to 2016), with initialization dates indicated in panel titles. Rows show the (a),(b) California heatwave, (c),(d) European heatwave, (e),(f) U.S. heatwave, and (g),(h) East Asian heatwave. White boxes indicate the averaging areas used for Fig. 2. All case studies use model version CY45R1, except for the East Asia heatwave, which uses CY46R1.

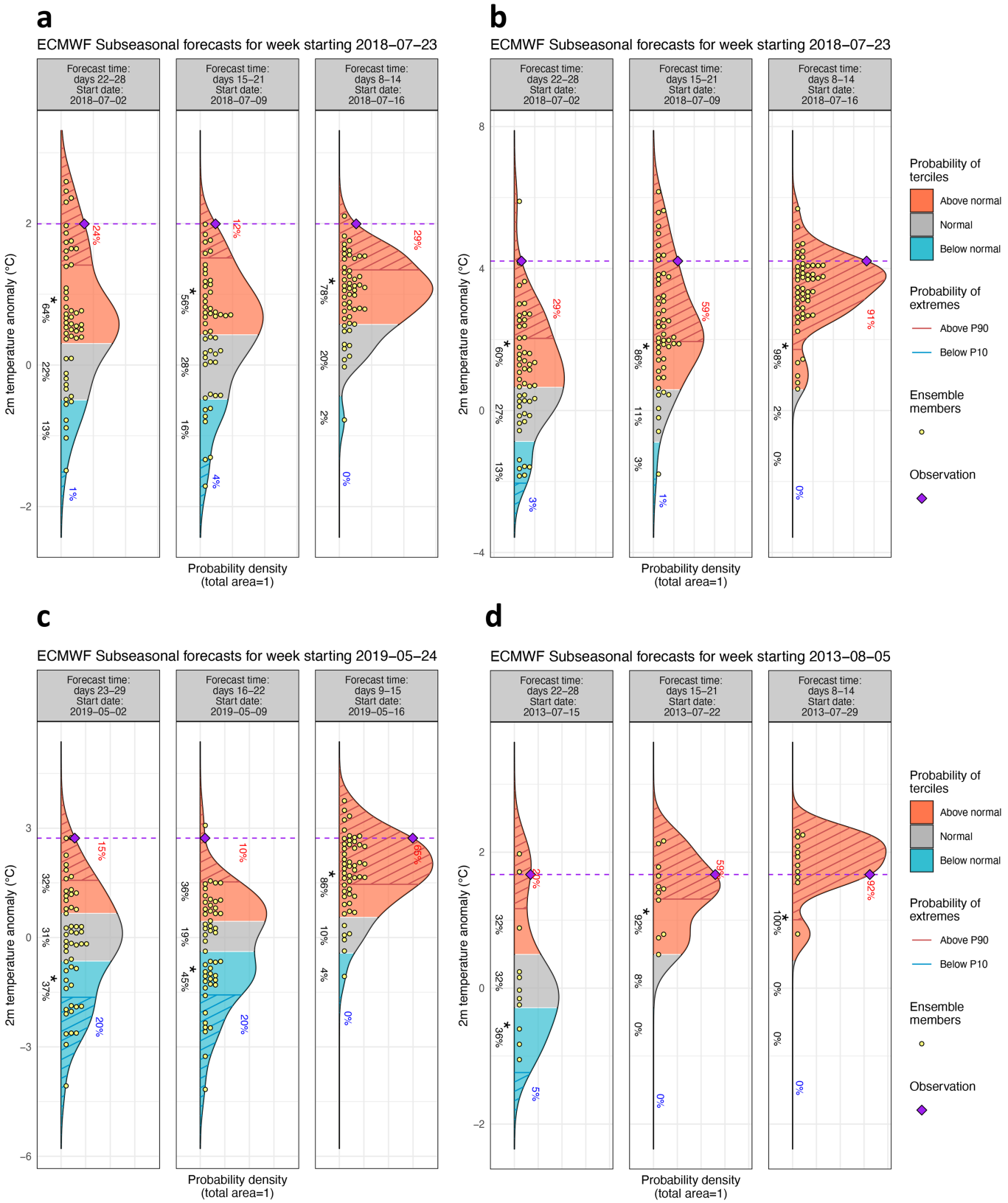

Fig. 2. Heatwaves: PDF of the predicted 2-m temperature anomalies from the model ensemble averaged over the target week (indicated in Table 1) for the heatwave case studies, averaged over the white boxes in Fig. 1 and initialized at (from left to right) 4, 3, and 2 weeks before the start of the target week. Panels show the (a) California heatwave 2018, (b) European heatwave 2018, (c) southeastern U.S. heatwave 2019, and (d) East Asian heatwave 2013. Tercile limits (below normal: blue; normal: gray; above normal: red) are computed with respect to the lead time–dependent model climatology. Values above the 66th percentile (below the 33rd percentile) are represented by red (blue) shading. Gray shading represents values between these terciles. The yellow dots indicate the ensemble members that were used to construct the PDF (51 for forecasts, 11 for hindcasts). The extremes above the 90th (below the 10th) percentile are hatched and their probabilities are indicated by red (blue) numbers. The purple dashed line represents the anomaly in ERA5 averaged over the target week.

Less than a year after the devastating 2018 heatwave, another series of heatwaves affected the United States in 2019. In late May 2019 (we here consider the week of 24–30 May), an early season heatwave affected the southeastern United States, tied to a wavy jet stream pattern with anomalously high (low) pressure over the southeastern (southwestern) United States (Di Liberto 2019). The model captures the temperature anomalies at 3 weeks' lead time, but it notably underestimates the extreme temperature anomalies (Figs. 1e,f), which is also found in the NCEP CFSv2 model (Luo and Zhang 2012). This underestimation is evident in the ensemble spread (Fig. 2c).

A further devastating heatwave was observed in East Asia in August 2013. The heatwave persisted for over 2 weeks from late July to mid-August, resulting in severe socioeconomic losses in the region (Duan et al. 2013; Sun et al. 2014; Li et al. 2019). South Korea experienced the hottest summer nights and the second-hottest summer days since 1954 (Min et al. 2014). In western Japan, daily maximum temperature records were broken or tied at 143 weather stations (JMA 2013), many of which were broken again during the 2018 heatwave. The extreme persistence and severity of the event resulted from the combination of a westward extension of the North Pacific subtropical high (Peng 2014; Li et al. 2015) and a zonal wave train (Yeo et al. 2019) resembling the circumglobal teleconnection (Ding and Wang 2005).

For the considered target week of 5–11 August 2013, a warm anomaly of over 4°C was observed in the large metropolitan areas of eastern China, while the heatwave extended to the Korean Peninsula and Japan (Fig. 1g). The temperature anomaly was larger in the urban areas than in rural areas (Wang et al. 2017), possibly due to the urban heat island effect. The temperature distribution is well captured by the model over land at a 3-week lead time, though the magnitude is slightly underestimated, while the warm anomaly over the eastern China Sea is not reproduced (Fig. 1h). When initialized four weeks before the target period on 15 July, more than a third of the ensemble members point to below-normal temperatures, although 20% already predict temperatures above the 90th percentile (Fig. 2d). However, starting at the 3-week lead time, essentially all ensemble members predict above-normal temperatures, and only one ensemble member at 2 weeks' lead time predicts temperatures below the 90th percentile. More importantly, the ensemble mean of these initializations quantitatively well captures the observations (i.e., individual ensemble members are well centered about the observed value). This result indicates that the 2013 East Asia heatwave is quantitatively well predicted by the model at a maximum lead time of 3 weeks.

Cold spells. Several examples of extreme cold spells in Europe are studied in this section. We start with a cold spell in eastern and southeastern Europe in late winter and early spring of 2003 (Levinson and Waple 2004) that preceded a record-breaking summer heatwave. The month of February was the coldest on record in Albania and Macedonia, and temperatures in southeastern Europe were between –2° and –5°C below normal for much of February and early March (Dittmann et al. 2004). The target week of 3–9 April (Fig. 3a) marked the end of this cold period, but was cold enough that the month of April registered record minimum temperatures in the Baltic region, the Danube watershed, and part of Italy and the Balkans (Dittmann et al. 2004). The extreme cold was associated with atmospheric blocking over the United Kingdom leading to southward advection of cold air masses from the Arctic, reaching southeastern Europe on 7 April. The temperature contrasts between the frigid air mass and the southern Adriatic Sea caused strong convective precipitation, with heavy snowfall along the coasts of western Greece, Albania, and southern Italy.

The model predicts the cold anomaly in central Europe (Fig. 3b), though with a southeastward shift and smaller anomalies than observed. The ensemble starts encompassing the observed anomaly at the 3-week lead time (19 March initialization, Fig. 4a), indicating a

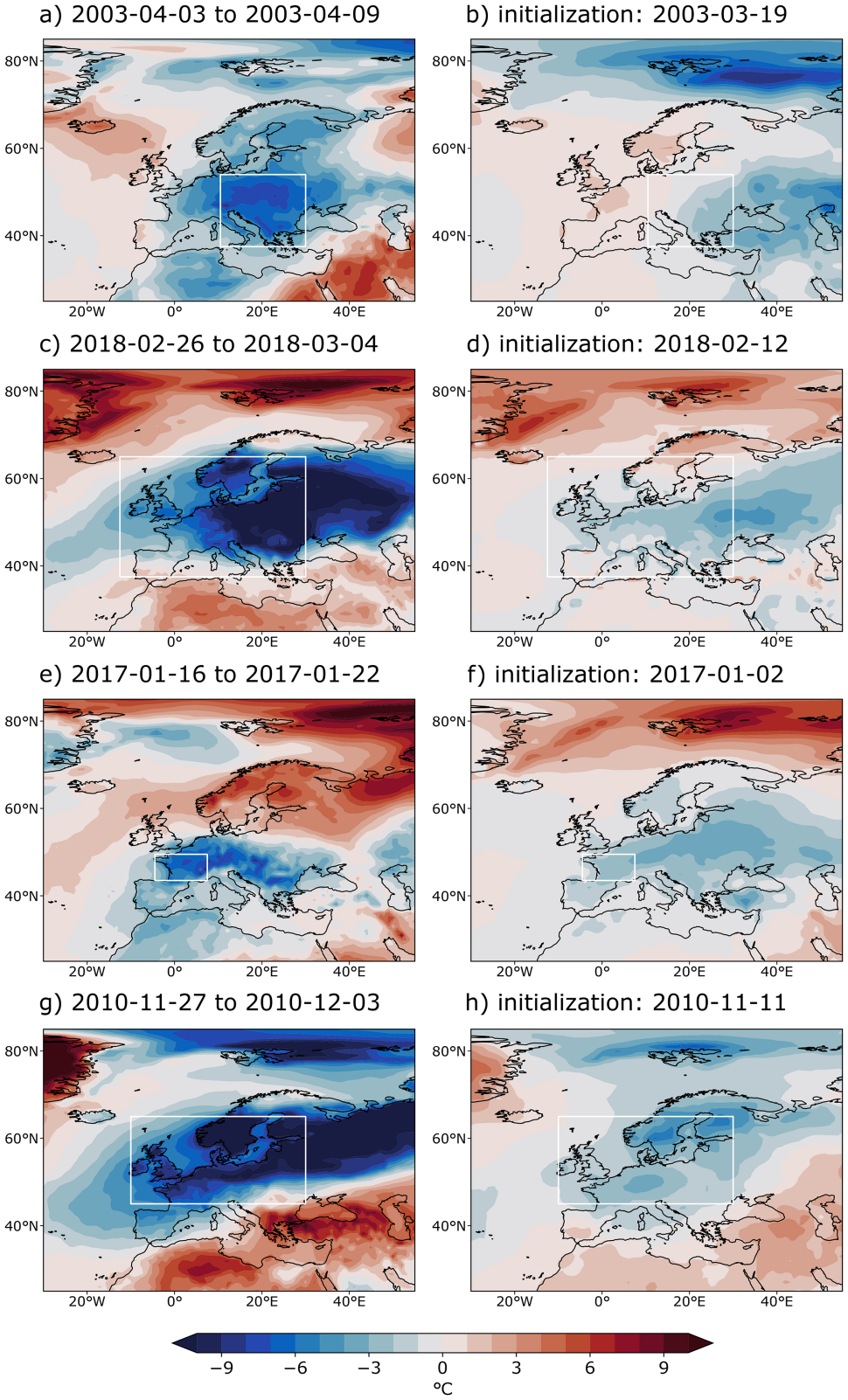

Fig. 3. As in Fig. 1, but for the cold spell case studies: (a),(b) Southeastern European cold spell in 2003 (model version CY46R1), (c),(d) central/northern European cold spell in 2018 (model version CY43R3), (e),(f) France cold spell in 2017 (model version CY43R1), and (g),(h) northern European cold spell in 2010 (model version CY46R1).

51% probability of temperatures in the lower tercile for the target week, and a 29% chance of temperatures below the 10th percentile. At the 2-week lead time, the confidence about the occurrence of cold weather is clearly increased, with 72% of the ensemble members indicating temperatures below normal, and 53% below the 10th-percentile threshold.

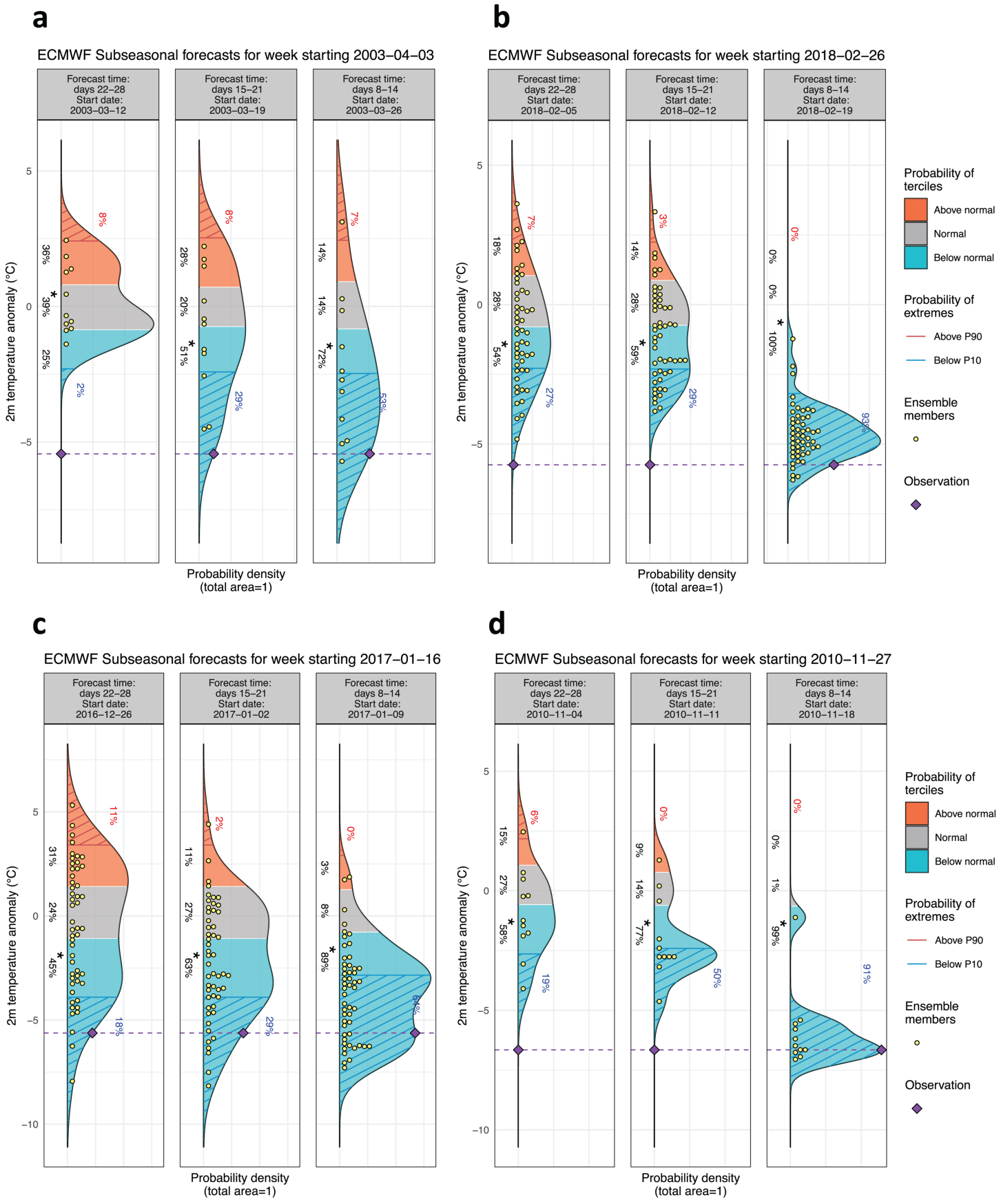

Fig. 4. As in Fig. 2, but for the cold spell case studies: (a) Southeastern European cold spell in 2003, (b) European cold spell in 2018, (c) France cold spell in 2017, and (d) the northern European cold spell in 2010.

Another cold spell preceding a hot summer occurred in late February/early March 2018 in central and western Europe after an otherwise mild winter. The cold wave was likely linked to a major SSW event in mid-February 2018, which enhanced the probability of the negative NAO and Greenland blocking during the peak of the cold event (Kautz et al. 2020). The SSW itself was anticipated 10 days ahead (Karpechko et al. 2018)—a typical predictability time scale for SSWs (Domeisen et al. 2020a). Knight et al. (2021) identified the extreme MJO event of January 2018 as an important driver of this SSW.

The blocking associated with this cold spell shows predictability in the ECMWF system (Ferranti et al. 2019). The forecast initialized on 12 February 2018, the day of the SSW event (a lead time of around 3 weeks), captures the cold anomaly over central Europe and part of the British Isles, but the anomaly is significantly underestimated (Figs. 3c,d). Already at 4 weeks lead time (initialization on 5 February) the most likely category is the below-normal tercile (with 54% of ensemble members) for temperature over western Europe (Fig. 4b). Further analysis using North Atlantic weather regimes suggests that the sequence of weather regimes before and during the cold spell [positive NAO, blocking, followed by negative NAO, as documented in Kautz et al. (2020)] were correctly anticipated by the model from the 12 February start date (not shown).

Another cold spell linked to atmospheric blocking occurred in winter 2016/17 (Fig. 3e). The block over Europe brought warm air to Scandinavia and Arctic air to eastern–central Europe in the second week of January (Magnusson 2017). A cutoff low developed, causing exceptionally low temperatures in the Balkan Peninsula as well as snowfall in Greece and southern Italy with significant socioeconomic impacts due to the long duration of the event (Anagnostopoulou et al. 2017). The following week (16–22 January 2017), central Europe was affected by further cold-air advection due to a tripole in surface pressure, with high pressure from the United Kingdom toward the Black Sea, and low pressure in the western Mediterranean and to the north of Scandinavia. This tripole was consistent with quiescent, cold, and dry conditions over central Europe in the region of the anticyclone (Fig. 3e).

The forecast issued on 2 January (3 weeks' lead time) already indicates an enhanced probability of below-normal temperatures (Fig. 3f). Four weeks before the event, the probability for temperatures in the lower tercile already reaches 45% and increases to 63% (89%) at 3 (2) weeks before the event (Fig. 4c). The ensemble clearly narrows toward the observed anomaly at shorter lead times. The probability of temperature anomalies below the 10th percentile increases closer to the event, from 18% (4 weeks before), to 29% (3 weeks before), and finally to 64% 2 weeks before the event.

The cold spell produced a peak in electricity demand, particularly in France, where most of the heating is powered by electricity. The concomitant low wind speeds led to a lower-than-normal wind power generation, and several nuclear power plants in France were under maintenance (RTE 2017). This combination caused a high-risk situation for France's energy system that could have been better managed given the forecasts, for example, through a postponement of the planned maintenance operations in the nuclear power plants.

Another extreme cold spell occurred in late 2010. From late November to early December 2010, Germany and France recorded the coldest December in 40 years, while in the United Kingdom this was the coldest December in 100 years (Fig. 3g). December 2010 was characterized by an unusually strong negative NAO (Maidens et al. 2013) with strong cold-air advection from northern Europe and Siberia (Prior and Kendon 2011). The cold anomaly over land was accompanied by a marine cold-air outbreak [MCAO; according to the MCAO index used in Afargan-Gerstman et al. (2020)] in the Norwegian and the Barents Seas. MCAOs can have devastating impacts on marine infrastructure and offshore activities, for example, by creating favorable conditions for the formation of polar lows (Rasmussen 1983; Kolstad et al. 2009; Noer et al. 2011; Landgren et al. 2019). Indeed, a polar low was detected in satellite imagery in the

Norwegian Sea off the coast of Norway on the 25 November 2010, 2 days before our selected target date, based on the STARS database of polar lows (http://polarlow.met.no/), but no records regarding damages from this polar low have been found. Although the occurrence of cold-air outbreaks in the North Atlantic and over northern Europe is often associated with stratospheric weak polar vortex events (e.g., Kolstad et al. 2010; Afargan-Gerstman et al. 2020), this event is unlikely to have been driven by the stratosphere, possibly reducing its predictability.

Cold anomalies had been predicted for northern Europe 3 weeks earlier by the hindcast initialized on 11 November; however, the prediction clearly underestimates the magnitude of the observed event (Figs. 3g,h). Hindcasts for lead times beyond 3 weeks (initialization on 4 November) already provide an indication of the cold anomaly, with probabilities around 20% for temperatures below the 10th percentile. Hindcasts initialized at lead times of 2 and 3 weeks capture the below-normal temperatures with a probability of above 90% and 50%, respectively (Fig. 4d). Hence, although the probability of a cold extreme is significantly increased already 3 weeks before the event, the magnitude of the extreme event is only captured at 2 weeks' lead time.

Precipitation events. In this section we focus on four events with anomalous precipitation in Central and South America, Europe, and Australia. The first considered event is analyzed in the context of a volcanic eruption, as an example of using subseasonal forecasts for compound events, where the possibility of heavy rainfall was a concern. Guatemala's Volcán de Fuego, a stratovolcano, erupted on 3 June 2018, killing at least 113 people, while more than 300 remained unaccounted for (Global Volcanism Program 2018). Ash plumes and pyroclastic flow material affected communities up to 25 km away from the volcano. The pyroclastic flows produced lahars (i.e., mudflow or debris flow) intermittently for several weeks, leading to evacuations of the nearby communities and displacing thousands of Guatemalans, destroying infrastructure and damaging crops. Overall, the eruption impacted 1.2 million Guatemalans, and cost more than $219 million (U.S. dollars; CEPAL 2018; CONRED 2018; WorldBank 2018).

The impacts could have been worse if precipitation, which typically peaks in the region in June, had been higher. Intense or persistent rainfall events (i) tend to make lahar viscosity thinner, which sustains the flow of pyroclastic debris for a longer duration, potentially causing more damage; (ii) can remobilize unconsolidated pyroclastic deposits, causing posteruption lahars; (iii) can displace hanging slabs of solidified mud, debris, and boulders down steep slopes, with the potential to destroy infrastructure and kill people; and (iv) tend to interfere with evacuation, search and rescue, cleaning, and rebuilding operations. Due to the activities deployed at the time in Guatemala by the Columbia University World Project "Adapting Agriculture to Climate Today, for Tomorrow" (IRI 2018), the International Research Institute for Climate and Society and INSIVUMEH—the Guatemalan national meteorological agency—started working together immediately after the eruption to provide calibrated subseasonal rainfall forecasts from the prediction system to the national government and a wide variety of local institutions.

Calibrated rainfall NextGen forecasts (Muñoz et al. 2019) initialized on 4 June indicated low chances of exceeding the weekly median for the following 4 weeks for most of Guatemala (cf. to Figs. 5a,b; Figs. 6a,b), and further analysis for the location of interest helped INSIVUMEH advise government institutions on evacuation, search and rescue, and cleaning and rebuilding operations. Subsequent weekly forecast updates confirmed the original expected outcomes. These results build evidence on the advantages of using real-time subseasonal rainfall forecasts to help decision-makers during and after volcanic eruptions, and potentially other seismologic and compound environmental events. Using a combination of forecasts at multiple time scales is suggested to be an optimal practice in these cases, consistent with the "ready–set–go" approach (Goddard et al. 2014).

Another event of interest occurred in January 2016, when a series of heavy precipitation events affected northwestern South America, leading to widespread flooding in coastal northern Ecuador, especially in the Province of Esmeraldas. The flood displaced 120 families, left one casualty, and was the largest such event in 20 years (Davies 2016). The flooding was associated with an early onset of the heavy rainfalls and severe mesoscale convective systems (MCSs) that would normally not be expected until annual precipitation peaks in April/May (Mohr and Zipser 1996; Bendix et al. 2009). On 25 January, convective storms developed into an MCS with an extent of around 250 km over the western Andes foothills of the Esmeraldas River basin, a region of abundant low-level moisture bounded by the Andes. This heavy precipitation event was favored by interactions between the very strong El Niño event and an unusually persistent MJO in phases 2 and 3 (Pineda et al. 2021).

Weekly ensemble-mean rainfall anomaly hindcasts represent the spatial pattern of the anomalous precipitation extreme over the catchment over all lead times (Figs. 5c,d), with the best event identification for week 3 initialized on 28 December 2015 [i.e., the week-3 anomaly was closer to the observations as compared to week 2 (not shown)]. For the Esmeraldas River basin the ROC scores for week 3 range from 0.5 to 0.6 (Fig. 6c), indicating low to modest discrimination of the above-normal rainfall on 25 January. The Spearman rank correlations range from −0.25 to 0.25 (Fig. 6d); thus, based on the hindcast, the model performance is limited for the region where the extreme rainfall occurred at a lead time of

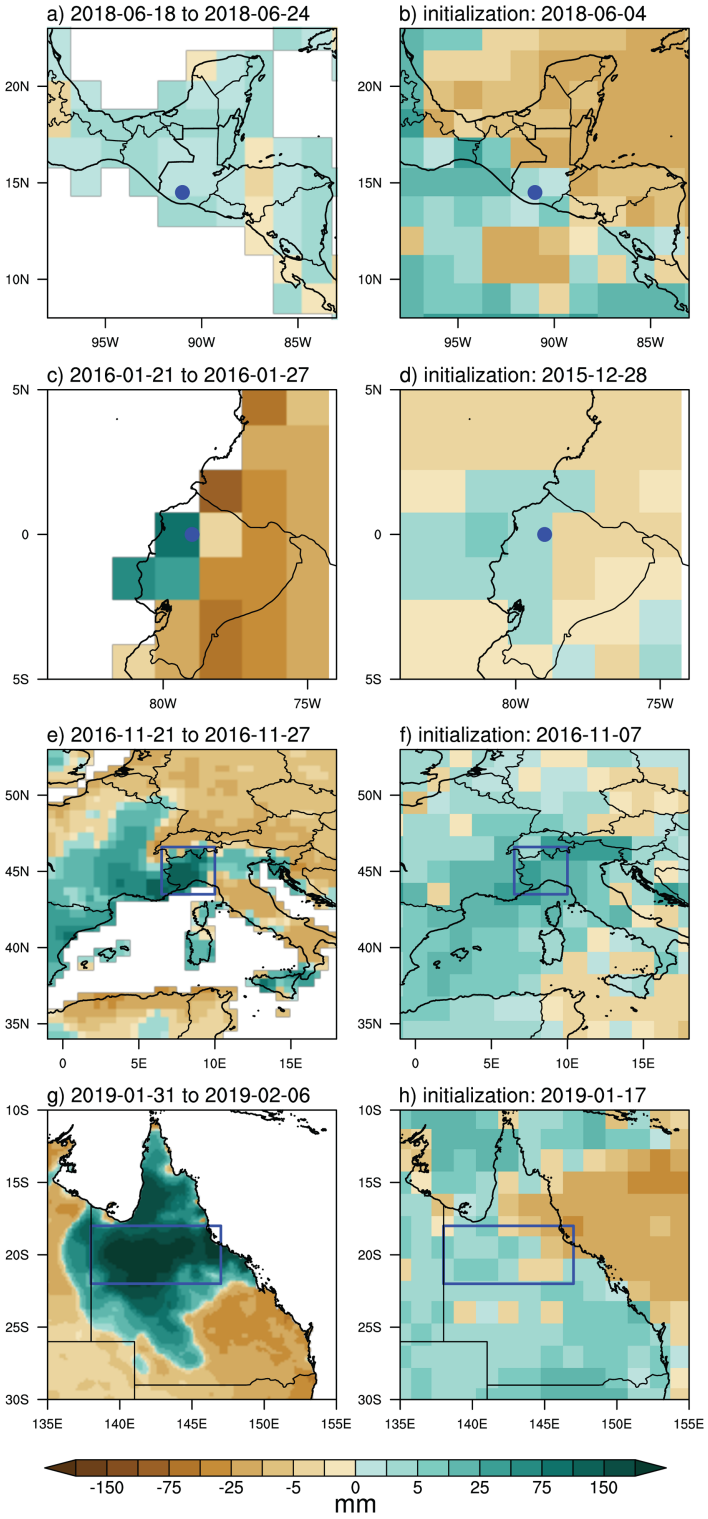

Fig. 5. Precipitation events: Accumulated precipitation anomalies over the target week (week 3, indicated in the panel titles) for (a),(c),(e),(g) observations and (b),(d),(f),(h) the ECMWF model prediction (initialization date indicated in the panel titles). Rows show (a),(b) Guatemala, (c),(d) western Ecuador, (e),(f) northwestern Italy, and (g),(h) northeastern Australia. The blue boxes and dots indicate the target location for each case study, as indicated in Table 1. Observations are from (a),(c),(e) CPC and (g) AWAP.

3 weeks. However, the positive precipitation anomaly of more than one standard deviation averaged over the grid points closest to the catchment was captured for all lead times of 1–3 weeks (Pineda et al. 2021). Therefore, the use of the S2S rainfall forecast could have provided decision-makers with useful information about the onset of this extreme precipitation event. A timely uptake of the available forecasts 2–3 weeks in advance by the National Met-Hydro Service could have allowed for an early warning for this catastrophic flood event.

Another heavy precipitation event affected northwestern Italy (Piedmont and Liguria) in the period from 21 to 25 November 2016. Over these 5 days, more than 50% of annual precipitation was recorded in several areas, with peaks above 600 mm (ARPA Liguria 2017; ARPA Piemonte 2017). Severe damage was caused by river floods with flow-rate return times up to 200 years, and widespread occurrence of shallow landslides (Cremonini and Tiranti 2018). This episode developed in the middle of a persistent drought affecting most of central and western Europe in 2016/17 (García-Herrera et al. 2019). The precipitation anomaly is underestimated by the model and exhibits a misplaced maximum for the forecast initialized on 7 November 2016 for week 3 (lead times of 15–21 days, Figs. 5e,f). However, the positive anomaly over northwestern Italy is reproduced more than 2 weeks in advance. Positive anomalies were also correctly located in the western Mediterranean region. These anomalies are significantly different at the 10% level from the ensemble climatology according to a Wilcoxon–Mann–Whitney test (not shown).

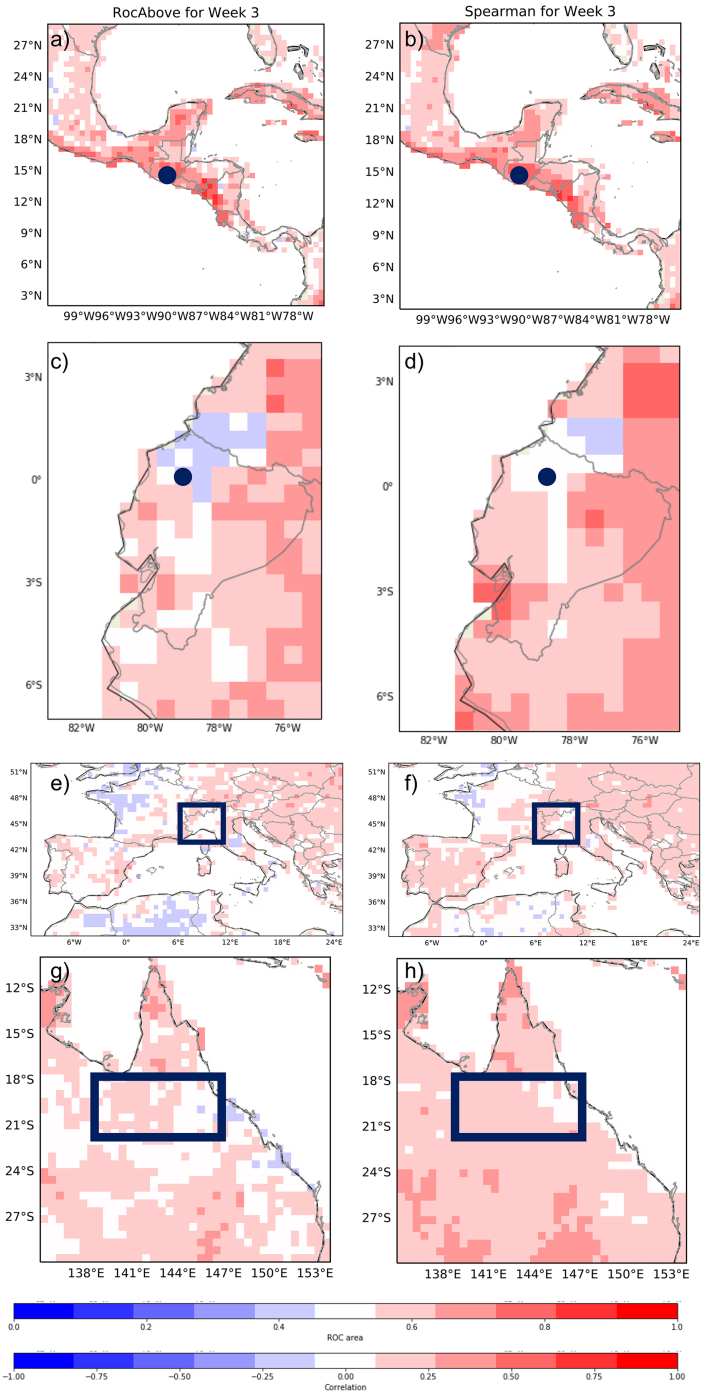

Fig. 6. Precipitation extremes: Predictability scores for week 3, (a),(c),(e),(g) assessed through the area under the ROC curve for the above-normal category and (b),(d),(f),(h) Spearman's rank correlation coefficient. The results were interpolated to the CPC unified grid. For details of the scores, see "Data and methods" section. Rows show (a),(b) Guatemala, (c),(d) western Ecuador, (e),(f) northwestern Italy, and (g),(h) northeastern Australia. The blue boxes and dots are as in Fig. 5.

The large-scale midtropospheric configuration leading to this precipitation event was characterized by a persistent low pressure anomaly over the Iberian Peninsula, surrounded

by areas of high pressure extending from the North Atlantic to eastern Europe (ARPA Piemonte 2017). This dipole in pressure anomalies favors meridional moist advection across the complex orography downstream, leading to heavy precipitation in the Mediterranean in this season (e.g., Buzzi et al. 2014; Khodayar et al. 2018). The anomalous persistence of the large-scale pattern likely favored the predictability of the event (Vitart et al. 2019). Although the verification scores of the week-3 forecasts for this area (Figs. 6e,f) indicate, on average, a relatively low predictive performance, the sufficiently correct representation of the atmospheric dipole in the extended range may have enhanced the predictability of precipitation for this event. Similarities are found with the historical Piedmont 1994 flood (Davolio et al. 2020), when heavy precipitation was triggered by a similar but less persistent large-scale pattern.

The last precipitation extreme considered here investigates extreme rainfall, strong winds, and below-normal daytime temperatures over tropical northeastern Australia in early February 2019. The event caused widespread infrastructure damage, coastal inundation to homes, and destroyed over 500,000 livestock, predominantly beef cattle (losses were in the dark green areas in Fig. 5g). The total economic loss was estimated at $5.68 billion AUD (Deloitte 2019). The extreme rainfall was associated with a quasi-stationary monsoon depression that lasted around 10 days, with weekly rainfall totals above 1,000 mm in some locations, maximum temperatures of 8°–12°C below average, and sustained winds between 30 and 40 km h^{-1} (Bureau of Meteorology 2019). The event was associated with an active MJO that stalled over the western Pacific (Cowan et al. 2019). Even though most of the predictability in extreme austral summer precipitation for northeastern Australia comes from equatorial Pacific SSTs (King et al. 2014), ENSO conditions were neutral and likely did not contribute to this event. Consistent with the neutral ENSO conditions, the Australian Bureau of Meteorology issued a monthly rainfall outlook for February with little indication of the impending event. Only in the week prior to the event, the Bureau's dynamical prediction system, the Australian Community Climate and Earth-System Simulator–Seasonal version 1 (ACCESS-S1), predicted a more-than-doubled likelihood of extreme rainfall (Cowan et al. 2019).

The operational real-time forecasts initialized on 17 January 2019 (i.e., a week-3 forecast) confirm the above analysis (Fig. 5h). The region with the highest observed rainfall accumulations (blue box in Fig. 5g) has a ROC score between 0.4 and 0.6, indicating low model performance (Fig. 6g). Likewise, widespread Spearman-rank correlations of between 0 and 0.25 (Fig. 6h) provide further evidence that the week-3 forecast does not predict the extreme rainfall week. This confirms separate results from eleven S2S models that suggest the rainfall event's very extreme nature could not be predicted with certainty more than a week ahead (not shown).

Cyclones. We here analyze the subseasonal predictability of four cyclones (three tropical cyclones and one medicane). While all selected tropical cyclones occurred in different regions, all were associated with an active MJO, as discussed below.

As a first case we investigate TC Claudia (Fig. 7a) in the western part of the Australian basin classified as a severe TC on the Australian scale. TCs in the western part of the Australian basin represent an important challenge to the oil industry since the majority of Australian oil rigs are located in this region. Therefore, the predictability of tropical cyclones a few weeks in advance in western Australia has important economic value, as well as societal impact in the case of landfall. Climatologically, 5.2 cyclones occur in that subbasin per season, with 2.6 reaching severe TC intensity and 1.2 making landfall in Australia (Chand et al. 2019). The Australian TC season typically lasts from November to April, with a peak in January to March. Claudia's characteristics (e.g., lifetime, latitude of genesis, maximum intensity, and dissipation) were very typical of western Australia TCs (Chand et al. 2019). Claudia developed

over Indonesia's Maluku Island on 4 January 2020 and moved southwestward along the northwestern coast of Australia for about 2 weeks (including a period as a tropical depression) (Figs. 7a,b). It reached a peak intensity of 968 hPa (140 km h^{-1}) on 13 January.

The prediction system initialized on 30 December 2019 predicted probabilities of up to 40% for a TC northwest of Australia for lead times of 15–21 days (week 3) (Fig. 7b)—significantly higher than the climatological probability (about 5%) for this season. Although the observed TC track is located slightly north of the area of maximum probability, this result suggests that the forecast could have provided a useful early warning for this TC. While other models from the S2S database also predicted an increased risk of TC activity in this region, the multimodel ensemble probability of TC strike was only around 10%–20%. Claudia coincided with an exceptionally intense MJO (three standard deviations above climatology of the RMM index; Wheeler and Hendon 2004) over the Maritime Continent and warm SST anomalies over the eastern Indian Ocean. This combination is likely to have contributed to make this intense and long-lasting tropical cyclone more predictable than usual.

Another recent example of a well-predicted system is Cyclone Belna (Fig. 7c) just a few weeks earlier. Belna formed to the north of the Mozambique Channel and eventually moved southward. Cyclones occur in the channel on average twice per year (Kolstad 2021). Over recent years, multiple tropical cyclones made landfall in that region (Idai and Kenneth in 2018/19 and Chalane, Eloise, Guambe, and Iman in 2020/21), leading to devastating floods in Mozambique and neighboring countries (Emerton et al. 2020).

For Cyclone Belna (Fig. 7c), the model prediction initialized on 18 November predicts a probability of cyclone occurrence of up to 30% in the Mozambique Channel at the remarkable lead time of 4 weeks (Fig. 7d). On 5 December, 17 days after forecast initialization, the system was upgraded to a tropical storm and named. On 7 December it attained hurricane intensity, and a day later it passed near the Mayotte Islands in the northernmost part of the channel. It made landfall in Madagascar on 9 December, to the east of the predicted path (Fig. 7d), and it dissipated over land 2 days later. A reason for the successful long-range prediction of Belna is likely the strong MJO envelope within which Belna formed (letter B in Fig. 8c), although the MJO was not successfully predicted thereafter. The model forecast (Fig. 8d) indicates enhanced convection in that area, particularly in early December when Belna developed. The very intense TC Ambali (letter A in Fig. 8c) also formed near the MJO envelope just to the east of Belna.

Another TC associated with an intense MJO event occurred during a period of unusually high TC activity in the western Pacific. In early June 2015, an MJO convective envelope developed over the Indian Ocean, intensified, and propagated eastward reaching an amplitude of 2.58 in the Real-time OLR MJO Index (ROMI) (Kiladis et al. 2014). Only two other MJO events during June and July in the period 1979–2018 reached this amplitude. This MJO event provided favorable conditions for TC formation leading to the genesis of Typhoons Linfa, Chan-hom (Fig. 7e), and Nangka over the western North Pacific, exemplified by the observed OLR anomalies and MJO-filtered OLR anomalies (Fig. 8a). Typhoons Linfa, Chan-hom, and Nangka (denoted by letters L, C, and N) in late June and early July formed soon after the passage of the MJO envelope. All three storms would go on to make landfall; Chan-hom was responsible for the second-highest damages [$1.5 billion (U.S. dollars)] in the west Pacific that season (Camargo 2016). Additional TCs in both the Indian Ocean and the western Pacific were associated with this MJO event (Fig. 8a).

The ensemble forecast initialized at 0000 UTC 15 June 2015 (Fig. 7f) indicates the increased probability of a TC during week 4 of the forecast (valid 7–13 July) in this area. The tracks of Typhoons Linfa, Chan-hom, and Nangka (from west to east) overlap this area of enhanced TC formation probability. The forecast also captures the eastward propagation of the MJO envelope (Fig. 8b), although the MJO amplitude is weaker than observed.

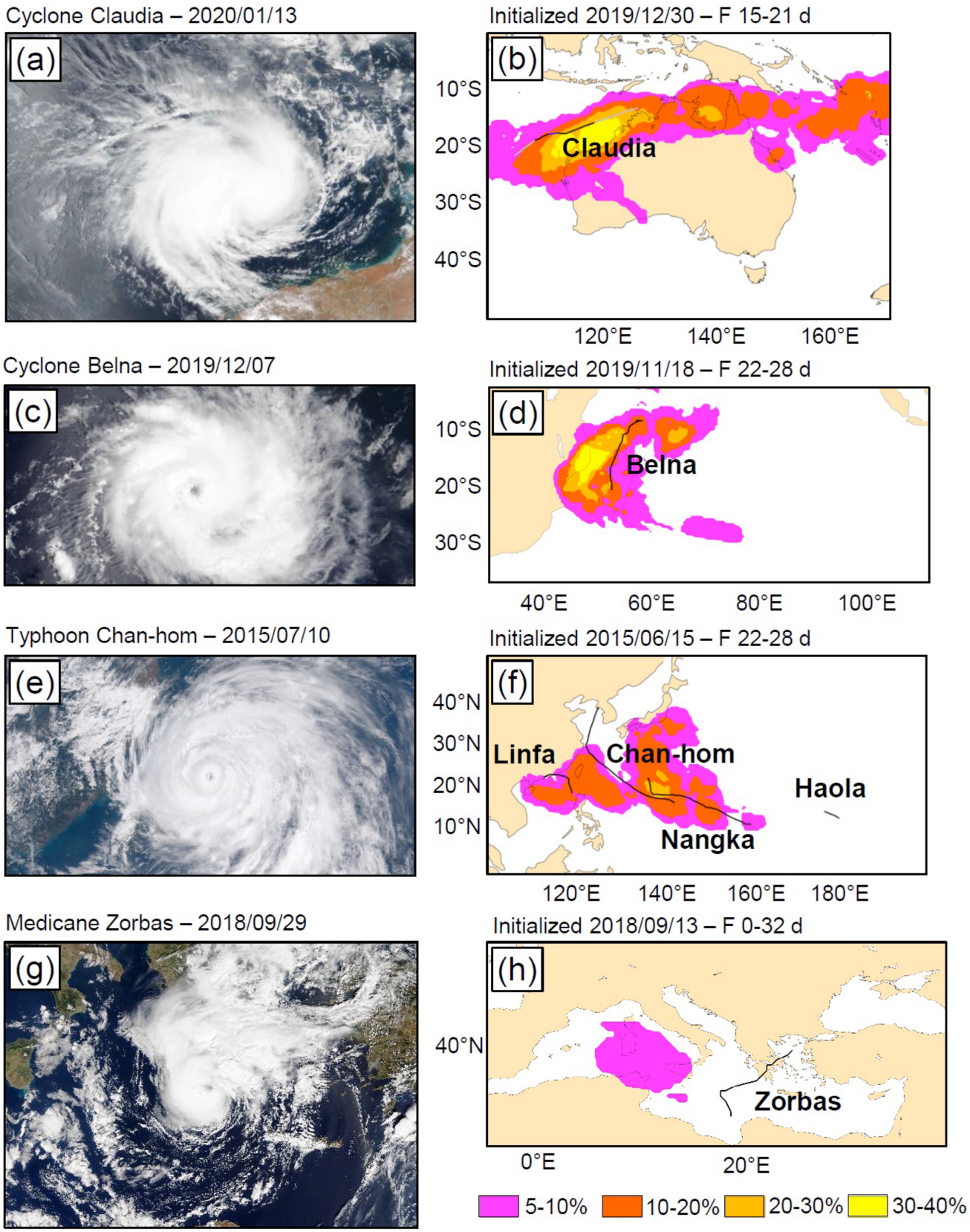

Fig. 7. Cyclones: Satellite images at a time close to the maximum intensity of the storms for (a) Cyclone Claudia on 13 Jan 2020 (NOAA) (c) Cyclone Belna on 7 Dec 2019 (NASA), (e) Typhoon Chan-hom on 10 Jul 2015 (SSEC/CIMSS, University of Wisconsin–Madison), and (g) Medicane Zorbas (2018M02) on 29 Sep 2018 (MODIS NASA). (b),(d),(f),(h) Probability of cyclone occurrence for (b) Claudia initialized on 30 Dec 2019 for lead times of 15–21 days, (d) Belna initialized on 18 Nov 2019 for lead times of 22–28 days, (f) Chan-hom initialized on 15 Jun 2015 for lead times of 22–28 days, and (h) Medicane Zorbas initialized on 13 Sep 2018 for lead times of 0–32 days. Black lines indicate the observed cyclone tracks during the verification period, and the names of the cyclones corresponding to the tracks are indicated. The different choice of lead times for the case studies refers to the longest lead time for which the events were possible to be predicted.

As a last case we investigate a medicane, specifically the Mediterranean Cyclone 2018–M02 Zorbas (Fig. 7g). The medicane developed on 27 September 2018 in the eastern Mediterranean Sea between Sicily and southern Greece and gradually intensified, developing characteristics of a tropical cyclone. As for many medicanes, its origin was related to a potential vorticity streamer (Miglietta et al. 2017). On 29 September, the storm made landfall at peak intensity in Kalamata, Peloponnese, Greece, with a pressure of 989 hPa and sustained winds of

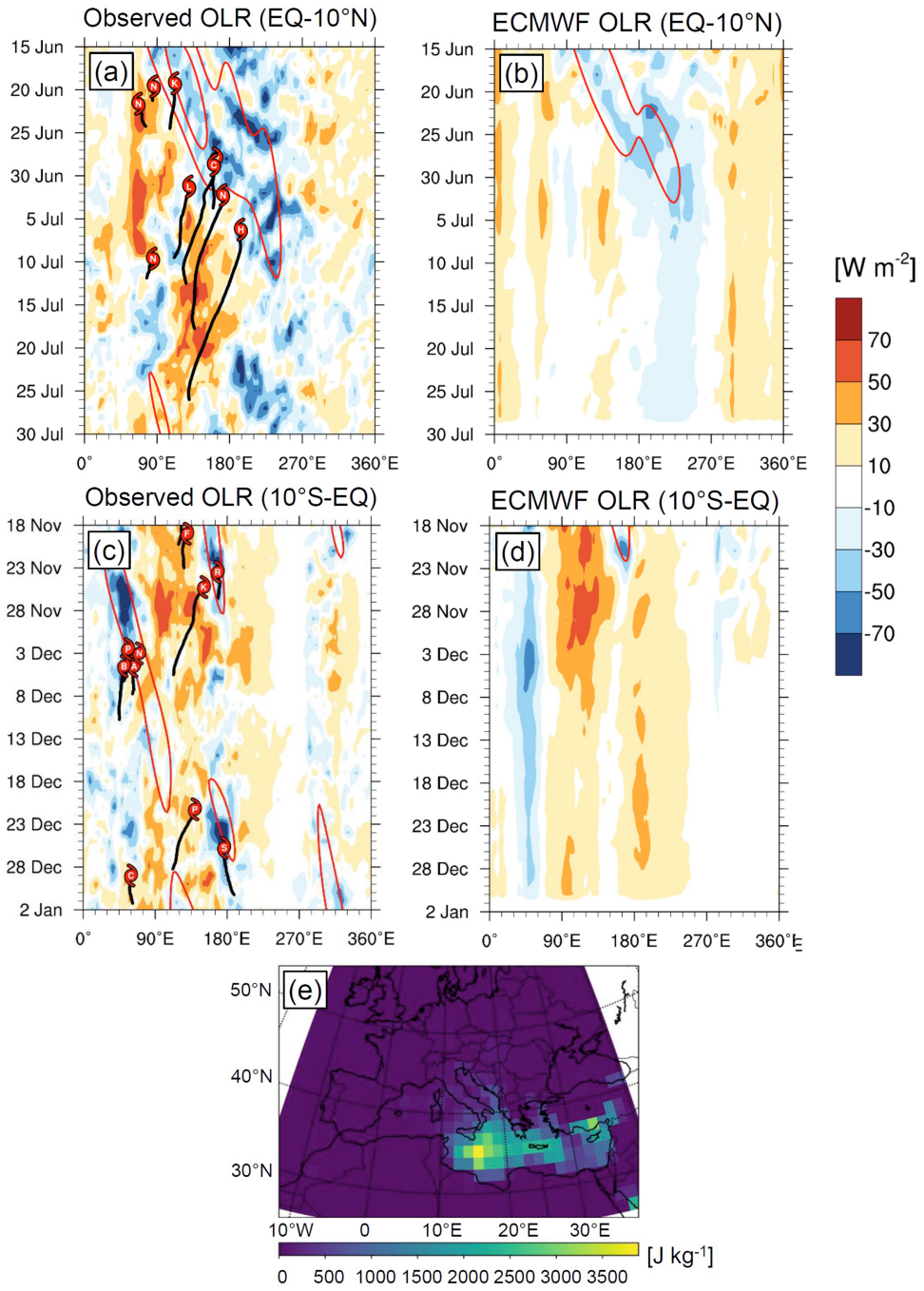

Fig. 8. Cyclones: Outgoing longwave radiation (OLR) anomalies (shaded; W m^{-2}) and MJO-filtered OLR anomalies (red contours; every 15 W m^{-2} for negative values) from (a),(c) observations averaged over (a) 0°–10°N and (c) 0°–10°S with tropical cyclone tracks (black lines) and names (first letter of the cyclone name in the red circle) and (b),(d) ECMWF ensemble forecasts initialized on 15 Jun 2015 and 18 Nov 2019. MJO filtering is performed using a wavenumber–frequency filter that selects for wavenumbers 0–9 and periods of 20–100 days. MJO-filtered OLR was calculated by padding the forecast with observations prior to initialization following the methodology described in Janiga et al. (2018). (e) CAPE (J kg^{-1}) from the ECMWF ensemble forecast initialized on 30 Aug 2018 and valid on 26 Sep 2018.

120 km h^{-1} (approximately 33 m s^{-1}). The event was associated with a Dvorak number of T4.0 (Hellenic National Meteorological Service 2019; ECMWF 2019), corresponding to a marginal category 1 hurricane.

The initialization on 13 September 2018 predicts a region of formation shifted to the west compared to the actual area of event formation (Gulf of Sirte, Libya) (Fig. 7h). While the low probability of formation is an indication of the difficulty of predicting such a rare event, the climatological probability of cyclone formation in the model in this region is less than 1%; hence, the displayed chance of a cyclone in this region is clearly above the expected probability. In addition, the prediction shows low probability for the event to follow the observed path (black line) toward Greece. One of the reasons for the limited predictability of the event was likely the uncertainty in the initial conditions near an upper-level jet streak over the Gulf of Saint Lawrence (Portmann et al. 2020).

However, predictability may potentially be improved using CAPE (see "Data and methods" section). For an initialization of the model as early as 30 August 2018 and a validation on 26 September 2018, very high values of CAPE are found in the formation region of Medicane Zorbas (Fig. 8). Hence, CAPE provides evidence of a medicane 3–4 weeks prior to its formation. Further analysis is needed to assess the full predictability capabilities of CAPE for medicanes.

General discussion and outlook

We have here demonstrated subseasonal predictability for selected case studies of some of the most prominent and impactful extreme events globally, namely, heatwaves, cold spells, precipitation events, and cyclones. Heatwaves tend to be the most predictable among the extreme events considered. The prediction system can often anticipate the anomalous temperature 3–4 weeks in advance, though often with a reduced amplitude. Cold spells also often show an indication of predictability, generally at lead times of 2–3 weeks. Precipitation events tend to be less predictable, but if the large-scale circulation associated with a large-scale driver (e.g., an active MJO) is successfully captured, predictability of 2–3 weeks can be obtained. For tropical cyclones, their formation region and tracks can often be anticipated 3 weeks in advance provided a successful prediction of strong MJO events. Furthermore, CAPE shows promise for indicating tracks and formation regions for extratropical cyclones. Note that these conclusions are based on the here documented case studies, and although the predictability and conclusions obtained here agree with other published results, it is likely that individual events may be more or less predictable depending on the region, type, and magnitude of the event. Therefore, in addition to differences in predictability between different types of extremes there are important differences in predictability within the same event type. In the here demonstrated case studies, these interevent differences hint at different processes and precursors responsible for forcing, modulating, or amplifying certain extreme events of the same type, including remote drivers such as the MJO.

We would like to emphasize that the case studies presented here do not represent a comprehensive evaluation; hence, the predictability shown for these events may differ from a systematic evaluation across a larger number of events. Hence, while this study only investigates a limited number of extreme events as case studies, systematic studies of interevent differences in predictability will be required to better understand the role of the identified drivers. In particular, extreme events with a common remote driver could be cross compared in order to more clearly evaluate the driver's role (or, in fact, its absence). These studies should also include an investigation of false alarms, that is, extreme events triggered by remote drivers and predicted in the model that do not verify in observations.

An improved process understanding of the drivers of extremes and their representation in prediction systems as well as the development of postprocessing techniques will continue to

significantly benefit the subseasonal prediction of extreme events. On the other hand, even with significant model improvements, many extremes will retain an inherent unpredictability related to the chaotic nature of the climate system. Still, understanding why and when certain extreme events are more predictable than others will help to identify and use windows of opportunity, that is, atmospheric states with enhanced predictability. Event-based and region-specific knowledge of the level of predictability of the relevant processes and the related extreme events will significantly benefit stakeholders and users of extreme weather data.

While this study has focused on a single prediction system from the ECMWF, an increasing number of multimodel studies for the prediction of specific extremes are currently becoming available (e.g., Y. Li et al. 2021; Materia et al. 2020; Domeisen et al. 2020b), highlighting intermodel differences rather than interevent differences, which were the focus of this study. Furthermore, bias correction and calibration methodologies that refine the forecast's statistical properties based on a reference period will further enhance these forecasts. In this study we used anomalies in order to correct the systematic bias and model drift, keeping in mind that this might affect the chance of the model to predict, for example, hot versus cold spells, especially for longer lead times. However, region- and process-specific biases and drifts are likely still present in our analysis. In addition, standard bias correction applied here is "unfair" (Risbey et al. 2021), since it uses observed data that would not be available to a real-time forecast: in fact, in several cases the observations used for the climatology occur after the forecast starts, and the hindcast therefore contains artificial skill. This can be misleading for users who must take decisions using real forecasts, which are likely to exhibit lower forecast skill than what is commonly shown in research studies.

In addition, a wider range of model evaluation and bias correction techniques are available, with the most relevant choices depending on the variable and on the desired characteristics for the output [see Torralba et al. (2017) and Manzanas et al. (2019) for a comparison of methodologies for seasonal predictions and Wernli et al. (2008) and Dorninger et al. (2018) for forecast evaluation techniques on deterministic time scales]. Although some standard methods and tools are starting to be used more widely (Muñoz 2020; Muñoz et al. 2019), implementation at subseasonal time scales is nontrivial and requires a robust climatological reference to be successful (Manrique-Suñén et al. 2020). One of the challenges is the limited amount of model data available for the reference period (short hindcast periods and few ensemble members). Examples of implementation of bias-correction methodologies for subseasonal predictions can be found in Monhart et al. (2018) and Manrique-Suñén et al. (2020). These statistical adjustments are of particular importance in sectoral applications (Materia et al. 2020; DeMott et al. 2021; DiSera et al. 2020), when S2S predictions are used as input in impact models to calculate sector-relevant indicators or derived variables (e.g., energy production or agricultural yield; White et al. 2022). As S2S predictions increasingly make their way into risk-based decision-making contexts, a continued development and assessment of subseasonal models, calibration techniques, and combination with other tools will significantly benefit these applications (Goddard et al. 2014; White et al. 2022).

Last, it remains difficult to quantify the economic value of S2S forecasts. In fact, even for very skillful forecasts, there can be significant economic losses that depend on factors beyond the forecasts themselves, involving the emergency response and preparedness of the affected region. However, it is clear that skillful forecasts on subseasonal to seasonal time scales can indeed add economic value, as has been shown for both temperature and cyclone predictions (Dorrington et al. 2020; Emanuel et al. 2012).

In summary, this work is meant to showcase the importance of subseasonal forecasts in the development and improvement of a large variety of climate services. Therefore, it is difficult to homogenize across event type, forecast quality metrics, and prediction format (deterministic versus probabilistic). By their own nature, distinct events in different locations

of the world require different verification tools, and time aggregations must be meaningful to users. This study goes toward this direction by starting to address the recommendations for advancing the S2S forecast verification practices recently highlighted by Coelho et al. (2019): Appropriate verification methods to deal with extreme events, novel verification measures specifically adapted for S2S forecasts, and enlargement of the sample size to address sampling uncertainties. All of these techniques are meant to build knowledge about the strengths and weaknesses of forecasts, and eventually increase confidence in S2S products among forecasters and users (Coelho et al. 2018).

As the performance of prediction models for extreme events at subseasonal lead times continues to increase with improvements in the understanding of extreme events and their representation in models, the here documented extreme events can be viewed as demonstrations and examples of this progress, which reaches far beyond these case studies, contributing to build or strengthen (depending on the case) a robust ecosystem of climate services (Goddard et al. 2020).

Acknowledgments. Support from the Swiss National Science Foundation through Project PP00P2_170523 to D.D., H.A.-G., and O.W. is gratefully acknowledged. In addition, support from the Swiss National Science Foundation through Project PP00P2_198896 to D.D. is gratefully acknowledged. H.A.-G. also acknowledges funding from the European Union's Horizon 2020 research and innovation programme under the Marie Skłodowska-Curie Grant Agreement 891514. Á.G.M., C.G.R., and D.P. were partially supported by the Columbia World Project "ACToday," at Columbia University in the city of New York (https://iri.columbia.edu/actoday/); Á.G.M. was also partially supported by the NOAA Grant NA18OAR4310275. A.M.-S., L.L, L.P., H.B., P.G., A.C.-P., D.B., and A.S. acknowledge funding from the European Union's Horizon 2020 research and innovation programme under Grant 7767874 (S2S4E). SJC acknowledges support of NOAA S2S Project NA16OAR4310079. TC is supported by the Northern Australian Climate Program (NACP). D.T. and H.M. are supported by the National Institute of Food and Agriculture Hatch project (Accession 1012578). S.-W.S. and H.K. are supported by the Basic Science Research Program through the National Research Foundation of Korea (2017R1E1A1A01074889). L.E.P acknowledges support of Corporación Ecuatoriana para el Desarrollo de la Investigación y la Academia (CEPRA grant). We acknowledge the use of the CSTools software package (Perez-Zanon et al. 2019) and R (R Core Team 2015) to produce Figs. 2 and 4.

Data availability statement. ERA5 data were obtained from the Copernicus Climate Change Service Climate Data Store (CDS), https://cds.climate.copernicus.eu/cdsapp#!/home. The ECMWF S2S model data were obtained through the MARS archive (https://apps.ecmwf.int/datasets/data/s2s/). CPC Global Unified Precipitation data were provided by the NOAA/OAR/ESRL/PSL, Boulder, Colorado, from their website at www.psl.noaa.gov/thredds/catalog/Datasets/cpc_global_precip/catalog.html. Australian precipitation data from the Australian Water Availability Project (AWAP) are available on request from the Bureau of Meteorology at www.bom.gov.au/climate/austmaps/metadata-daily-rainfall.shtml. The satellite image for Tropical Cyclone Claudia was captured by *NOAA-20* satellite's IITS instrument (www.nesdis.noaa.gov/content/tropical-cyclone-claudia-loses-strength-it-moves-away-australia). The satellite image for Cyclone Belna was obtained from https://en.wikipedia.org/wiki/Cyclone_Belna (NASA: https://worldview.earthdata.nasa.gov/). The satellite image for Typhoon Chan-hom was obtained from https://en.wikipedia.org/wiki/Typhoon_Chan-hom_%282015%29 (SSEC/CIMSS, University of Wisconsin–Madison). The satellite image for Medicane Zorbas is a MODIS image captured by NASA's *Terra* satellite (EOSDIS Worldview) from https://commons.wikimedia.org/wiki/File:Zorbas_2018-09-29_0912Z.jpg. The ECMWF CAPE data for studying Medicane Zorbas were obtained from the IRI/LDEO Climate Data Library (https://iridl.ldeo.columbia.edu/SOURCES/.ECMWF/.S2S). Observed tropical cyclone data are obtained from the International Best Track Archive for Climate Stewardship (IBTrACS) (Knapp et al. 2010) at https://climatedataguide.ucar.edu/climate-data/ibtracs-tropical-cyclone-best-track-data.

References

Afargan-Gerstman, H., I. Polkova, L. Papritz, P. Ruggieri, M. P. King, P. J. Athanasiadis, J. Baehr, and D. I. Domeisen, 2020: Stratospheric influence on North Atlantic marine cold air outbreaks following sudden stratospheric warming events. *Wea. Climate Dyn.*, **1**, 541–553, https://doi.org/10.5194/wcd-1-541-2020.

Albergel, C., and Coauthors, 2019: Monitoring and forecasting the impact of the 2018 summer heatwave on vegetation. *Remote Sens.*, **11**, 520, https://doi.org/10.3390/rs11050520.

Alexander, L. V., M. Bador, R. Roca, S. Contractor, M. G. Donat, and P. L. Nguyen, 2020: Intercomparison of annual precipitation indices and extremes over global land areas from in situ, space-based and reanalysis products. *Environ. Res. Lett.*, **15**, 055002, https://doi.org/10.1088/1748-9326/ab79e2.

Anagnostopoulou, C., K. Tolika, G. Lazoglou, and P. Maheras, 2017: The exceptionally cold January of 2017 over the Balkan Peninsula: A climatological and synoptic analysis. *Atmosphere*, **8**, 252, https://doi.org/10.3390/atmos8120252.

ARPA Liguria, 2017: Rapporto di evento meteoidrologico del 20–25/11/2016. ARPA Liguria Tech. Rep., 25 pp.

ARPA Piemonte, 2017: Gli eventi alluvionali in Piemonte—Evento del 21–25 novembre 2016. ARPA Piemonte Tech. Rep., 273 pp.

Auffhammer, M., P. Baylis, and C. H. Hausman, 2017: Climate change is projected to have severe impacts on the frequency and intensity of peak electricity demand across the United States. *Proc. Natl. Acad. Sci. USA*, **114**, 1886–1891, https://doi.org/10.1073/pnas.1613193114.

Bauer, P., A. Thorpe, and G. Brunet, 2015: The quiet revolution of numerical weather prediction. *Nature*, **525**, 47–55, https://doi.org/10.1038/nature14956.

Bayr, T., D. I. V. Domeisen, and C. Wengel, 2019: The effect of the equatorial Pacific cold SST bias on simulated ENSO teleconnections to the North Pacific and California. *Climate Dyn.*, **53**, 3771–3789, https://doi.org/10.1007/s00382-019-04746-9.

Beerli, R., H. Wernli, and C. M. Grams, 2017: Does the lower stratosphere provide predictability for month-ahead wind electricity generation in Europe? *Quart. J. Roy. Meteor. Soc.*, **143**, 3025–3036, https://doi.org/10.1002/qj.3158.

Bendix, J., K. Trachte, J. Cermak, R. Rollenbeck, and T. Nauß, 2009: Formation of convective clouds at the foothills of the tropical eastern Andes (south Ecuador). *J. Appl. Meteor. Climatol.*, **48**, 1682–1695, https://doi.org/10.1175/2009JAMC2078.1.

Berg, A., and J. Sheffield, 2018: Climate change and drought: The soil moisture perspective. *Curr. Climate Change Rep.*, **4**, 180–191, https://doi.org/10.1007/s40641-018-0095-0.

Bloomfield, H., D. J. Brayshaw, L. Shaffrey, P. J. Coker, and H. E. Thornton, 2018: The changing sensitivity of power systems to meteorological drivers: A case study of Great Britain. *Environ. Res. Lett.*, **13**, 054028, https://doi.org/10.1088/1748-9326/aabff9.

——, C. Suitters, and D. Drew, 2020: Meteorological drivers of European power system stress. *J. Renewable Energy*, **2020**, 5481010, https://doi.org/10.1155/2020/5481010.

Brás, T. A., J. Seixas, N. Carvalhais, and J. Jägermeyr, 2021: Severity of drought and heatwave crop losses tripled over the last five decades in Europe. *Environ. Res. Lett.*, **16**, 065012, https://doi.org/10.1088/1748-9326/abf004.

Brunner, L., N. Schaller, J. Anstey, J. Sillmann, and A. K. Steiner, 2018: Dependence of present and future European temperature extremes on the location of atmospheric blocking. *Geophys. Res. Lett.*, **45**, 6311–6320, https://doi.org/10.1029/2018GL077837.

Buizza, R., and Coauthors, 2017: IFS cycle 43r3 brings model and assimilation updates. *ECMWF Newsletter*, No. 152, ECMWF, Reading, United Kingdom, 18–22, www.ecmwf.int/node/18193.

Bunzel, F., W. A. Mueller, M. Dobrynin, K. Froehlich, S. Hagemann, H. Pohlmann, T. Stacke, and J. Baehr, 2018: Improved seasonal prediction of European summer temperatures with new five-layer soil-hydrology scheme. *Geophys. Res. Lett.*, **45**, 346–353, https://doi.org/10.1002/2017GL076204.

Bureau of Meteorology, 2019: An extended period of heavy rainfall and flooding in tropical Queensland. Bureau of Meteorology Special Climate Statement 69, 47 pp., www.bom.gov.au/climate/current/statements/scs69.pdf.

Buzzi, A., S. Davolio, P. Malguzzi, O. Drofa, and D. Mastrangelo, 2014: Heavy rainfall episodes over Liguria in autumn 2011: Numerical forecasting experiments. *Nat. Hazards Earth Syst. Sci.*, **14**, 1325–1340, https://doi.org/10.5194/nhess-14-1325-2014.

Camargo, S. J., 2016: Western North Pacific basin [in "State of the Climate in 2015"]. *Bull. Amer. Meteor. Soc.*, **97** (8), S110–S113, https://doi.org/10.1175/2016BAMSStateoftheClimate.1.

——, and S. Hsiang, 2015: Tropical cyclones: From the influence of climate to their socio-economic impacts. *Extreme Events: Observations, Modeling and Economics*, *Geophys. Monogr.*, Vol. 214, Amer. Geophys. Union, 303–342.

——, M. C. Wheeler, and A. H. Sobel, 2009: Diagnosis of the MJO modulation of tropical cyclogenesis using an empirical index. *J. Atmos. Sci.*, **66**, 3061–3074, https://doi.org/10.1175/2009JAS3101.1.

——, and Coauthors, 2019: Tropical cyclone prediction on subseasonal time-scales. *Trop. Cyclone Res. Rev.*, **8**, 150–165, https://doi.org/10.1016/j.tcrr.2019.10.004.

——, F. Vitart, C.-Y. Lee, and M. K. Tippett, 2021: Skill, predictability, and cluster analysis of Atlantic tropical storms and hurricanes in the ECMWF monthly forecasts. *Mon. Wea. Rev.*, **149**, 3781–3802, https://doi.org/10.1175/MWR-D-21-0075.1.

Camp, J., and Coauthors, 2018: Skilful multi-week tropical cyclone prediction in ACCESS-S1 and the role of the MJO. *Quart. J. Roy. Meteor. Soc.*, **144**, 1337–1351, https://doi.org/10.1002/qj.3260.

Campbell, S., T. A. Remenyi, C. J. White, and F. H. Johnston, 2018: Heatwave and health impact research: A global review. *Health Place*, **53**, 210–218, https://doi.org/10.1016/j.healthplace.2018.08.017.

Carrera, M. L., R. W. Higgins, and V. E. Kousky, 2004: Downstream weather impacts associated with atmospheric blocking over the northeast Pacific. *J. Climate*, **17**, 4823–4839, https://doi.org/10.1175/JCLI-3237.1.

Cavicchia, L., H. von Storch, and S. Gualdi, 2014: A long-term climatology of medicanes. *Climate Dyn.*, **43**, 1183–1195, https://doi.org/10.1007/s00382-013-1893-7.

CEPAL, 2018: ECLAC team assesses impact of Volcán de Fuego eruption in Guatemala. CEPAL Tech. Rep. 8, 6 pp.

Chand, S. S., and Coauthors, 2019: Review of tropical cyclones in the Australian region: Climatology, variability, predictability and trends. *Wiley Interdiscip. Rev.: Climate Change*, **10**, e602, https://doi.org/10.1002/wcc.602.

Charlton-Perez, A. J., L. Ferranti, and R. W. Lee, 2018: The influence of the stratospheric state on North Atlantic weather regimes. *Quart. J. Roy. Meteor. Soc.*, **144**, 1140–1151, https://doi.org/10.1002/qj.3280.

——, R. W. Aldridge, C. M. Grams, and R. Lee, 2019: Winter pressures on the UK health system dominated by the Greenland blocking weather regime. *Wea. Climate Extremes*, **25**, 100218, https://doi.org/10.1016/j.wace.2019.100218.

——, W. T. K. Huang, and S. H. Lee, 2021: Impact of sudden stratospheric warmings on United Kingdom mortality. *Atmos. Sci. Lett.*, **22**, e1013, https://doi.org/10.1002/asl.1013.

Chen, M., W. Shi, P. Xie, V. B. Silva, V. E. Kousky, R. Wayne Higgins, and J. E. Janowiak, 2008: Assessing objective techniques for gauge-based analyses of global daily precipitation. *J. Geophys. Res.*, **113**, D04110, https://doi.org/10.1029/2007JD009132.

Coelho, C. A., M. A. Firpo, and F. M. de Andrade, 2018: A verification framework for South American sub-seasonal precipitation predictions. *Meteor. Z.*, **27**, 503–520, https://doi.org/10.1127/metz/2018/0898.

——, B. Brown, L. Wilson, M. Mittermaier, and B. Casati, 2019: Forecast verification for S2S timescales. *Sub-Seasonal to Seasonal Prediction*, Elsevier, 337–361.

Cohen, J., and J. Jones, 2011: A new index for more accurate winter predictions. *Geophys. Res. Lett.*, **38**, L21701, https://doi.org/10.1029/2011GL049626.

CONRED, 2018: Informe erupción Volcán de Fuego. CONRED Tech. Rep., 8 pp.

Cowan, T., and Coauthors, 2019: Forecasting the extreme rainfall, low temperatures, and strong winds associated with the northern Queensland floods of

February 2019. *Wea. Climate Extremes*, **26**, 100232, https://doi.org/10.1016/j.wace.2019.100232.

Cradden, L. C., and F. McDermott, 2018: A weather regime characterisation of Irish wind generation and electricity demand in winters 2009–11. *Environ. Res. Lett.*, **13**, 054022, https://doi.org/10.1088/1748-9326/aabd40.

Cremonini, R., and D. Tiranti, 2018: The weather radar observations applied to shallow landslides prediction: A case study from north-western Italy. *Front. Earth Sci.*, **6**, 134, https://doi.org/10.3389/feart.2018.00134.

Davies, R., 2016: Ecuador—1 dead after floods and landslides—14cm of rain in 24 hours in Esmeraldas. FloodList, http://floodlist.com/america/ecuador-floods-esmeraldas-january-2016.

Davolio, S., P. Malguzzi, O. Drofa, D. Mastrangelo, and A. Buzzi, 2020: The Piedmont flood of November 1994: A testbed of forecasting capabilities of the CNR-ISAC meteorological model suite. *Bull. Atmos. Sci. Technol.*, **1**, 263–282, https://doi.org/10.1007/s42865-020-00015-4.

de Andrade, F. M., C. A. S. Coelho, and I. F. A. Cavalcanti, 2019: Global precipitation hindcast quality assessment of the Subseasonal to Seasonal (S2S) Prediction project models. *Climate Dyn.*, **52**, 5451–5475, https://doi.org/10.1007/s00382-018-4457-z.

DeFlorio, M. J., and Coauthors, 2019: Experimental subseasonal-to-seasonal (S2S) forecasting of atmospheric rivers over the western United States. *J. Geophys. Res. Atmos.*, **124**, 11 242–11 265, https://doi.org/10.1029/2019JD031200.

Deloitte, 2019: The social and economic cost of the north and far north Queensland Monsoon trough. Deloitte, www2.deloitte.com/au/en/pages/economics/articles/social-economic-cost-north-far-north-queensland-monsoon-trough.html.

DeMott, C., Á. G. Muñoz, C. D. Roberts, C. M. Spillman, and F. Vitart, 2021: The benefits of better ocean weather forecasting. *Eos*, **102**, https://eos.org/features/the-benefits-of-better-ocean-weather-forecasting.

de Vries, H., R. J. Haarsma, and W. Hazeleger, 2012: Western European cold spells in current and future climate. *Geophys. Res. Lett.*, **39**, L04706, https://doi.org/10.1029/2011GL050665.

Di Liberto, T. D., 2019: Heat wave broils the U.S. Southeast over Memorial Day weekend 2019. NOAA, www.climate.gov/news-features/event-tracker/heat-wave-broils-us-southeast-over-memorial-day-weekend-2019.

Ding, Q., and B. Wang, 2005: Circumglobal teleconnection in the Northern Hemisphere summer. *J. Climate*, **18**, 3483–3505, https://doi.org/10.1175/JCLI3473.1.

Dirmeyer, P. A., and Coauthors, 2018: Verification of land–atmosphere coupling in forecast models, reanalyses, and land surface models using flux site observations. *J. Hydrometeor.*, **19**, 375–392, https://doi.org/10.1175/JHM-D-17-0152.1.

DiSera, L., H. Sjödin, J. Rocklöv, Y. Tozan, B. Súdre, H. Zeller, and Á. G. Muñoz, 2020: The mosquito, the virus, the climate: An unforeseen Réunion in 2018. *GeoHealth*, **4**, e2020GH000253, https://doi.org/10.1029/2020GH000253.

Dittmann, E., P. Hechler, and P. Bissolli, 2004: Annual bulletin on the climate in WMO region VI—2003. DWD Tech. Rep., 94 pp., www.dwd.de/DE/leistungen/ravibulletinjahr/archiv/bulletin_2003.pdf?__blob=publicationFile&v=4.

Dobrynin, M., and Coauthors, 2018: Improved teleconnection-based dynamical seasonal predictions of boreal winter. *Geophys. Res. Lett.*, **45**, 3605–3614, https://doi.org/10.1002/2018GL077209.

Domeisen, D. I. V., 2019: Estimating the frequency of sudden stratospheric warming events from surface observations of the North Atlantic Oscillation. *J. Geophys. Res. Atmos.*, **124**, 3180–3194, https://doi.org/10.1029/2018JD030077.

——, and A. H. Butler, 2020: Stratospheric drivers of extreme events at the Earth's surface. *Commun. Earth Environ.*, **1**, 59, https://doi.org/10.1038/s43247-020-00060-z.

——, ——, K. Fröhlich, M. Bittner, W. Müller, and J. Baehr, 2015: Seasonal predictability over Europe arising from El Niño and stratospheric variability in the MPI-ESM seasonal prediction system. *J. Climate*, **28**, 256–271, https://doi.org/10.1175/JCLI-D-14-00207.1.

——, and Coauthors, 2020a: The role of the stratosphere in subseasonal to seasonal prediction: 1. Predictability of the stratosphere. *J. Geophys. Res. Atmos.*, **125**, e2019JD030920, https://doi.org/10.1029/2019JD030920.

——, and Coauthors, 2020b: The role of the stratosphere in subseasonal to seasonal prediction: 2. Predictability arising from stratosphere-troposphere coupling. *J. Geophys. Res. Atmos.*, **125**, e2019JD030923, https://doi.org/10.1029/2019JD030923.

Donat, M. G., A. L. Lowry, L. V. Alexander, P. A. O'Gorman, and N. Maher, 2016: More extreme precipitation in the world's dry and wet regions. *Nat. Climate Change*, **6**, 508–513, https://doi.org/10.1038/nclimate2941.

Dong, L., C. Mitra, S. Greer, and E. Burt, 2018: The dynamical linkage of atmospheric blocking to drought, heatwave and urban heat island in southeastern US: A multi-scale case study. *Atmosphere*, **9**, 33, https://doi.org/10.3390/atmos9010033.

Dorninger, M., E. Gilleland, B. Casati, M. P. Mittermaier, E. E. Ebert, B. G. Brown, and L. J. Wilson, 2018: The setup of the MesoVICT project. *Bull. Amer. Meteor. Soc.*, **99**, 1887–1906, https://doi.org/10.1175/BAMS-D-17-0164.1.

Dorrington, J., I. Finney, T. Palmer, and A. Weisheimer, 2020: Beyond skill scores: Exploring sub-seasonal forecast value through a case-study of French month-ahead energy prediction. *Quart. J. Roy. Meteor. Soc.*, **146**, 3623–3637, https://doi.org/10.1002/qj.3863.

Doss-Gollin, J., Á. G. Muñoz, S. J. Mason, and M. Pastén, 2018: Heavy rainfall in Paraguay during the 2015/16 austral summer: Causes and subseasonal-to-seasonal predictive skill. *J. Climate*, **31**, 6669–6685, https://doi.org/10.1175/JCLI-D-17-0805.1.

——, D. J. Farnham, U. Lall, and V. Modi, 2021: How unprecedented was the February 2021 Texas cold snap? *Environ. Res. Lett.*, **16**, 064056, https://doi.org/10.1088/1748-9326/ac0278.

Duan, H., S. Wang, and J. Feng, 2013: The national drought situation and its impacts and causes in the summer 2013. *J. Arid Meteor.*, **31**, 633–640.

Duchez, A., and Coauthors, 2016: Drivers of exceptionally cold North Atlantic Ocean temperatures and their link to the 2015 European heat wave. *Environ. Res. Lett.*, **11**, 074004, https://doi.org/10.1088/1748-9326/11/7/074004.

ECMWF, 2019: 201809—Rainfall—Zorbas. ECMWF Severe Event Catalogue, https://confluence.ecmwf.int/display/FCST/201809+-+Rainfall+-+Zorbas#app-switcher.

Emanuel, K., F. Fondriest, and J. Kossin, 2012: Potential economic value of seasonal hurricane forecasts. *Wea. Climate Soc.*, **4**, 110–117, https://doi.org/10.1175/WCAS-D-11-00017.1.

Emerton, R., and Coauthors, 2020: Emergency flood bulletins for Cyclones Idai and Kenneth: A critical evaluation of the use of global flood forecasts for international humanitarian preparedness and response. *Int. J. Disaster Risk Reduct.*, **50**, 101811, https://doi.org/10.1016/j.ijdrr.2020.101811.

Enomoto, T., 2004: Interannual variability of the Bonin high associated with the propagation of Rossby waves along the Asian jet. *J. Meteor. Soc. Japan*, **82**, 1019–1034, https://doi.org/10.2151/jmsj.2004.1019.

Evans, J. L., and R. J. Allan, 1992: El Niño/Southern Oscillation modification to the structure of the monsoon and tropical cyclone activity in the Australian region. *Int. J. Climatol.*, **12**, 611–623, https://doi.org/10.1002/joc.3370120607.

Ferranti, L., and P. Viterbo, 2006: The European summer of 2003: Sensitivity to soil water initial conditions. *J. Climate*, **19**, 3659–3680, https://doi.org/10.1175/JCLI3810.1.

——, L. Magnusson, F. Vitart, and D. S. Richardson, 2018: How far in advance can we predict changes in large-scale flow leading to severe cold conditions over Europe? *Quart. J. Roy. Meteor. Soc.*, **144**, 1788–1802, https://doi.org/10.1002/qj.3341.

——, ——, ——, and ——, 2019: A new product to flag up the risk of cold spells in Europe weeks ahead. *ECMWF Newsletter*, No. 158, ECMWF, Reading, United Kingdom, 15–20, www.ecmwf.int/node/18881.

Fischer, E. M., S. I. Seneviratne, P. L. Vidale, D. Lüthi, and C. Schär, 2007: Soil moisture–atmosphere interactions during the 2003 European summer heat wave. *J. Atmos. Sci.*, **20**, 5081–5099, https://doi.org/10.1175/JCLI4288.1.

Flaounas, E., S. Raveh-Rubin, H. Wernli, P. D. C. Dynamics, and N. Butchart, 2015: The dynamical structure of intense Mediterranean cyclones. *Climate Dyn.*, **44**, 2411–2427, https://doi.org/10.1007/s00382-014-2330-2.

——, S. L. Gray, and F. Teubler, 2021: A process-based anatomy of Mediterranean cyclones: From baroclinic lows to tropical-like systems. *Wea. Climate Dyn.*, **2**, 255–279, https://doi.org/10.5194/wcd-2-255-2021.

Ford, T. W., P. A. Dirmeyer, and D. O. Benson, 2018: Evaluation of heat wave forecasts seamlessly across subseasonal timescales. *npj Climate Atmos. Sci.*, **1**, 20, https://doi.org/10.1038/s41612-018-0027-7.

Fragkoulidis, G., V. Wirth, P. Bossmann, and A. H. Fink, 2018: Linking Northern Hemisphere temperature extremes to Rossby wave packets. *Quart. J. Roy. Meteor. Soc.*, **144**, 553–566, https://doi.org/10.1002/qj.3228.

Freychet, N., S. Tett, J. Wang, and G. Hegerl, 2017: Summer heat waves over eastern China: Dynamical processes and trend attribution. *Environ. Res. Lett.*, **12**, 024015, https://doi.org/10.1088/1748-9326/aa5ba3.

Gao, M., B. Wang, J. Yang, and W. Dong, 2018: Are peak summer sultry heat wave days over the Yangtze–Huaihe River basin predictable? *J. Climate*, **31**, 2185–2196, https://doi.org/10.1175/JCLI-D-17-0342.1.

García-Herrera, R., and Coauthors, 2019: The European 2016/17 drought. *J. Climate*, **32**, 3169–3187, https://doi.org/10.1175/JCLI-D-18-0331.1.

Gershunov, A., 1998: ENSO influence on intraseasonal extreme rainfall and temperature frequencies in the contiguous United States: Implications for long-range predictability. *J. Climate*, **11**, 3192–3203, https://doi.org/10.1175/1520-0442(1998)011<3192:EIOIER>2.0.CO;2.

——, and K. Guirguis, 2012: California heat waves in the present and future. *Geophys. Res. Lett.*, **39**, L18710, https://doi.org/10.1029/2012GL052979.

——, and ——, 2015: California heat waves, July 2015. CNAP Tech. Rep., 2 pp., www.swcasc.arizona.edu/sites/default/files/HeatWaves.pdf.

Global Volcanism Program, 2018: Report on Fuego (Guatemala). *Bull. Global Volcanism Network*, **43**, https://doi.org/10.5479/si.GVP.BGVN201808-342090.

Goddard, L., W. E. Baethgen, H. Bhojwani, and A. W. Robertson, 2014: The International Research Institute for Climate & Society: Why, what and how. *Earth Perspect.*, **1**, 10, https://doi.org/10.1186/2194-6434-1-10.

——, and Coauthors, 2020: Climate services ecosystems in times of COVID-19. *WMO Bull.*, **69**, 39–46, https://public.wmo.int/en/resources/bulletin/climate-services-ecosystems-times-of-covid-19.

Grazzini, F., and F. Vitart, 2015: Atmospheric predictability and Rossby wave packets. *Quart. J. Roy. Meteor. Soc.*, **141**, 2793–2802, https://doi.org/10.1002/qj.2564.

Gregory, P. A., J. Camp, K. Bigelow, and A. Brown, 2019: Sub-seasonal predictability of the 2017–2018 Southern Hemisphere tropical cyclone season. *Atmos. Sci. Lett.*, **20**, e886, https://doi.org/10.1002/asl.886.

Gruber, K., T. Gauster, L. Ramirez-Camargo, G. Laaha, and J. Schmidt, 2021: The Texas 2021 cold spell in a climate-power system perspective. *EGU General Assembly*, Online, EGU, EGU21-7180, https://doi.org/10.5194/egusphere-egu21-7180.

Hall, J. D., A. J. Matthews, and D. J. Karoli, 2001: The modulation of tropical cyclone activity in the Australian region by the Madden–Julian oscillation. *Mon. Wea. Rev.*, **129**, 2970–2982, https://doi.org/10.1175/1520-0493(2001)129<2970:TMOTCA>2.0.CO;2.

Hamill, T. M., and G. N. Kiladis, 2014: Skill of the MJO and Northern Hemisphere blocking in GEFS medium-range reforecasts. *Mon. Wea. Rev.*, **142**, 868–885, https://doi.org/10.1175/MWR-D-13-00199.1.

Hartmann, D. L., 2015: Pacific sea surface temperature and the winter of 2014. *Geophys. Res. Lett.*, **42**, 1894–1902, https://doi.org/10.1002/2015GL063083.

Hauser, M., R. Orth, and S. I. Seneviratne, 2016: Role of soil moisture versus recent climate change for the 2010 heat wave in western Russia. *Geophys. Res. Lett.*, **43**, 2819–2826, https://doi.org/10.1002/2016GL068036.

Hellenic National Meteorological Service, 2019: Significant weather and climate events in Greece 2018. HNMS Rep., 12 pp., www.hnms.gr/emy/en/pdf/2018_GRsignificantEVENT_en.pdf.

Hersbach, H., and Coauthors, 2020: The ERA5 global reanalysis. *Quart. J. Roy. Meteor. Soc.*, **146**, 1999–2049, https://doi.org/10.1002/qj.3803.

Hsiang, S., 2010: Temperatures and cyclones strongly associated with economic production in the Caribbean and Central America. *Proc. Natl. Acad. Sci. USA*, **107**, 15 367–15 372, https://doi.org/10.1073/pnas.1009510107.

——, and D. Narita, 2012: Adaptation to cyclone risk: Evidence from the global cross-section. *Climate Change Econ.*, **3**, 1250011, https://doi.org/10.1142/S201000781250011X.

Huang, W., and X. Liang, 2010: Convective asymmetries associated with tropical cyclone landfall: β-plane simulations. *Adv. Atmos. Sci.*, **27**, 795–806, https://doi.org/10.1007/s00376-009-9086-3.

IPCC, 2013: *Climate Change 2013: The Physical Science Basis.* Cambridge University Press, 1535 pp., https://doi.org/10.1017/CBO9781107415324.

IRI, 2018: Adapting Agriculture to Climate Today, for tomorrow (ACToday). Columbia Climate School, https://iri.columbia.edu/actoday.

Janiga, M., C. J. Schreck, J. A. Ridout, M. Flatau, N. P. Barton, E. J. Metzger, and C. A. Reynolds, 2018: Subseasonal forecasts of convectively coupled equatorial waves and the MJO: Activity and predictive skill. *Mon. Wea. Rev.*, **146**, 2337–2360, https://doi.org/10.1175/MWR-D-17-0261.1.

JMA, 2013: Extreme summer conditions in Japan in 2013. Japan Meteorological Agency Tokyo Climate Center Rep., 9 pp.

Jones, C., D. E. Waliser, K. M. Lau, and W. Stern, 2004: Global occurrences of extreme precipitation and the Madden–Julian oscillation: Observations and predictability. *J. Climate*, **17**, 4575–4589, https://doi.org/10.1175/3238.1.

Jones, D. A., W. Wang, and R. Fawcett, 2009: High-quality spatial climate data-sets for Australia. *Aust. Meteor. Oceanogr. J.*, **58**, 233–248, https://doi.org/10.22499/2.5804.003.

Karpechko, A. Y., A. Charlton-Perez, M. Balmaseda, N. Tyrrell, and F. Vitart, 2018: Predicting sudden stratospheric warming 2018 and its climate impacts with a multimodel ensemble. *Geophys. Res. Lett.*, **45**, 13 538–13 546, https://doi.org/10.1029/2018GL081091.

Kautz, L.-A., I. Polichtchouk, T. Birner, H. Garny, and J. G. Pinto, 2020: Enhanced extended-range predictability of the 2018 late-winter Eurasian cold spell due to the stratosphere. *Quart. J. Roy. Meteor. Soc.*, **146**, 1040–1055, https://doi.org/10.1002/qj.3724.

Kenyon, J., and G. C. Hegerl, 2010: Influence of modes of climate variability on global precipitation extremes. *J. Climate*, **23**, 6248–6262, https://doi.org/10.1175/2010JCLI3617.1.

Khodayar, S., N. Kalthoff, and C. Kottmeier, 2018: Atmospheric conditions associated with heavy precipitation events in comparison to seasonal means in the western Mediterranean region. *Climate Dyn.*, **51**, 951–967, https://doi.org/10.1007/s00382-016-3058-y.

Kiladis, G. N., J. Dias, K. H. Straub, M. C. Wheeler, S. N. Tulich, K. Kikuchi, K. M. Weickmann, and M. J. Ventrice, 2014: A comparison of OLR and circulation-based indices for tracking the MJO. *Mon. Wea. Rev.*, **142**, 1697–1715, https://doi.org/10.1175/MWR-D-13-00301.1.

Kim, Y.-H., S.-K. Min, D. A. Stone, H. Shiogama, and P. Wolski, 2018: Multi-model event attribution of the summer 2013 heat wave in Korea. *Wea. Climate Extremes*, **20**, 33–44, https://doi.org/10.1016/j.wace.2018.03.004.

King, A. D., N. P. Klingaman, L. V. Alexander, M. G. Donat, N. C. Jourdain, and P. Maher, 2014: Extreme rainfall variability in Australia: Patterns, drivers, and predictability. *J. Climate*, **27**, 6035–6050, https://doi.org/10.1175/JCLI-D-13-00715.1.

——, D. Hudson, E.-P. Lim, A. G. Marshall, H. H. Hendon, T. P. Lane, and O. Alves, 2020: Sub-seasonal to seasonal prediction of rainfall extremes in Australia. *Quart. J. Roy. Meteor. Soc.*, **146**, 2228–2249, https://doi.org/10.1002/qj.3789.

Knapp, K. R., M. C. Kruk, D. H. Levinson, H. J. Diamond, and C. J. Neumann, 2010: The International Best Track Archive for Climate Stewardship (IBTrACS) unifying tropical cyclone data. *Bull. Amer. Meteor. Soc.*, **91**, 363–376, https://doi.org/10.1175/2009BAMS2755.1.

Knight, J., and Coauthors, 2021: Predictability of European winters 2017/2018 and 2018/2019: Contrasting influences from the tropics and stratosphere. *Atmos. Sci. Lett.*, **22**, e1009, https://doi.org/10.1002/asl.1009.

Knutson, T., and Coauthors, 2019: Tropical cyclones and climate change assessment: Part I. Detection and attribution. *Bull. Amer. Meteor. Soc.*, **100**, 1987–2007, https://doi.org/10.1175/BAMS-D-18-0189.1.

——, and Coauthors, 2020: Tropical cyclones and climate change assessment: Part II. Projected response to anthropogenic warming. *Bull. Amer. Meteor. Soc.*, **101**, E303–E322, https://doi.org/10.1175/BAMS-D-18-0194.1.

Kolstad, E. W., 2021: Prediction and precursors of Idai and 38 other tropical cyclones and storms in the Mozambique Channel. *Quart. J. Roy. Meteor. Soc.*, **147**, 45–57, https://doi.org/10.1002/qj.3903.

——, T. J. Bracegirdle, and I. A. Seierstad, 2009: Marine cold-air outbreaks in the North Atlantic: Temporal distribution and associations with large-scale atmospheric circulation. *Climate Dyn.*, **33**, 187–197, https://doi.org/10.1007/s00382-008-0431-5.

——, T. Breiteig, and A. A. Scaife, 2010: The association between stratospheric weak polar vortex events and cold air outbreaks in the Northern Hemisphere. *Quart. J. Roy. Meteor. Soc.*, **136**, 886–893, https://doi.org/10.1002/qj.620.

Kornhuber, K., S. Osprey, D. Coumou, S. Petri, V. Petoukhov, S. Rahmstorf, and L. Gray, 2019: Extreme weather events in early summer 2018 connected by a recurrent hemispheric wave-7 pattern. *Environ. Res. Lett.*, **14**, 054002, https://doi.org/10.1088/1748-9326/ab13bf.

Koster, R. D., and Coauthors, 2010: Contribution of land surface initialization to subseasonal forecast skill: First results from a multi-model experiment. *Geophys. Res. Lett.*, **37**, L02402, https://doi.org/10.1029/2009GL041677.

Kueh, M.-T., and C.-Y. Lin, 2020: The 2018 summer heatwaves over northwestern Europe and its extended-range prediction. *Sci. Rep.*, **10**, 19283, https://doi.org/10.1038/s41598-020-76181-4.

Landgren, O. A., I. A. Seierstad, and T. Iversen, 2019: Projected future changes in marine cold-air outbreaks associated with polar lows in the northern North-Atlantic Ocean. *Climate Dyn.*, **53**, 2573–2585, https://doi.org/10.1007/s00382-019-04642-2.

Lee, C.-Y., S. J. Camargo, F. Vitart, A. H. Sobel, and M. K. Tippett, 2018: Subseasonal tropical cyclone genesis prediction and MJO in the S2S dataset. *Wea. Forecasting*, **33**, 967–988, https://doi.org/10.1175/WAF-D-17-0165.1.

——, ——, ——, ——, J. Camp, S. Wang, M. K. Tippett, and Q. Yang, 2020: Subseasonal predictions of tropical cyclone occurrence and ACE in the S2S dataset. *Wea. Forecasting*, **35**, 921–938, https://doi.org/10.1175/WAF-D-19-0217.1.

Lee, M., and T. Frisius, 2018: On the role of convective available potential energy (CAPE) in tropical cyclone intensification. *Tellus*, **70A**, 1–18, https://doi.org/10.1080/16000870.2018.1433433.

Lehtonen, I., and A. Y. Karpechko, 2016: Observed and modeled tropospheric cold anomalies associated with sudden stratospheric warmings. *J. Geophys. Res. Atmos.*, **121**, 1591–1610, https://doi.org/10.1002/2015JD023860.

Lenggenhager, S., and O. Martius, 2019: Atmospheric blocks modulate the odds of heavy precipitation events in Europe. *Climate Dyn.*, **53**, 4155–4171, https://doi.org/10.1007/s00382-019-04779-0.

Leroy, A., and M. C. Wheeler, 2008: Statistical prediction of weekly tropical cyclone activity in the Southern Hemisphere. *Mon. Wea. Rev.*, **136**, 3637–3654, https://doi.org/10.1175/2008MWR2426.1.

Levinson, D., and A. Waple, Eds., 2004: State of the Climate in 2003. *Bull. Amer. Meteor. Soc.*, **85** (6), S1–S72, https://doi.org/10.1175/1520-0477-85.6s.S1.

Li, C., F. Zwiers, X. Zhang, G. Li, Y. Sun, and M. Wehner, 2021: Changes in annual extremes of daily temperature and precipitation in CMIP6 models. *J. Climate*, **34**, 3441–3460, https://doi.org/10.1175/JCLI-D-19-1013.1.

Li, J., T. Ding, X. Jia, and X. Zhao, 2015: Analysis on the extreme heat wave over China around Yangtze River region in the summer of 2013 and its main contributing factors. *Adv. Meteor.*, **2015**, 706713, https://doi.org/10.1155/2015/706713.

Li, M., Y. Yao, D. Luo, and L. Zhong, 2019: The linkage of the large-scale circulation pattern to a long-lived heatwave over mideastern China in 2018. *Atmosphere*, **10**, 89, https://doi.org/10.3390/atmos10020089.

Li, Y., D. Tian, and H. Medina, 2021: Multimodel subseasonal precipitation forecasts over the contiguous United States: Skill assessment and statistical postprocessing. *J. Hydrometeor.*, **22**, 2581–2600, https://doi.org/10.1175/JHM-D-21-0029.1.

Lin, I.-I., and Coauthors, 2017: ENSO and tropical cyclones. *El Niño Southern Oscillation in a Changing Climate*, *Geophys. Monogr.*, Vol. 253, Amer. Geophys. Union, Wiley, 377–408.

Liu, X., B. He, L. Guo, L. Huang, and D. Chen, 2020: Similarities and differences in the mechanisms causing the European summer heatwaves in 2003, 2010, and 2018. *Earth's Future*, **8**, e2019EF001386, https://doi.org/10.1029/2019EF001386.

Lopez, H., R. West, S. Dong, G. Goni, B. Kirtman, S.-K. Lee, and R. Atlas, 2018: Early emergence of anthropogenically forced heat waves in the western United States and Great Lakes. *Nat. Climate Change*, **8**, 414–420, https://doi.org/10.1038/s41558-018-0116-y.

Luo, L., and Y. Zhang, 2012: Did we see the 2011 summer heat wave coming? *Geophys. Res. Lett.*, **39**, L09708, https://doi.org/10.1029/2012GL051383.

Magnusson, L., 2017: The cold spell in eastern Europe in January 2017. *ECMWF Newsletter*, No. 151, ECMWF, Reading, United Kingdom, 22–27, www.ecmwf.int/en/newsletter/151/news/cold-spell-eastern-europe-january-2017.

Maidens, A., A. Arribas, A. A. Scaife, C. MacLachlan, D. Peterson, and J. Knight, 2013: The influence of surface forcings on prediction of the North Atlantic Oscillation regime of winter 2010/11. *Mon. Wea. Rev.*, **141**, 3801–3813, https://doi.org/10.1175/MWR-D-13-00033.1.

Manrique-Suñén, A., N. Gonzalez-Reviriego, V. Torralba, N. Cortesi, and F. J. Doblas-Reyes, 2020: Choices in the verification of S2S forecasts and their implications for climate services. *Mon. Wea. Rev.*, **148**, 3995–4008, https://doi.org/10.1175/MWR-D-20-0067.1.

Manzanas, R., J. M. Gutiérrez, J. Bhend, S. Hemri, F. J. Doblas-Reyes, V. Torralba, E. Penabad, and A. Brookshaw, 2019: Bias adjustment and ensemble recalibration methods for seasonal forecasting: A comprehensive intercomparison using the C3S dataset. *Climate Dyn.*, **53**, 1287–1305, https://doi.org/10.1007/s00382-019-04640-4.

Mason, S., M. K. Tippet, L. Song, and A. G. Muñz, 2021: Climate Predictability Tool, version 17.4.4. Columbia University Academic Commons, https://doi.org/10.7916/d8-1bcm-8620.

Materia, S., Á. G. Muñoz, M. C. Álvarez-Castro, S. J. Mason, F. Vitart, and S. Gualdi, 2020: Multimodel subseasonal forecasts of spring cold spells: Potential value for the hazelnut agribusiness. *Wea. Forecasting*, **35**, 237–254, https://doi.org/10.1175/WAF-D-19-0086.1.

McKinnon, K. A., A. Rhines, M. P. Tingley, and P. Huybers, 2016: Long-lead predictions of eastern United States hot days from Pacific sea surface temperatures. *Nat. Geosci.*, **9**, 389–394, https://doi.org/10.1038/ngeo2687.

Merryfield, W. J., and Coauthors, 2020: Current and emerging developments in subseasonal to decadal prediction. *Bull. Amer. Meteor. Soc.*, **101**, E869–E896, https://doi.org/10.1175/BAMS-D-19-0037.1.

Merz, B., and Coauthors, 2020: Impact forecasting to support emergency management of natural hazards. *Rev. Geophys.*, **58**, e2020RG000704, https://doi.org/10.1029/2020RG000704.

Miglietta, M. M., D. Cerrai, S. Laviola, E. Cattani, and V. Levizzani, 2017: Potential vorticity patterns in Mediterranean "hurricanes." *Geophys. Res. Lett.*, **44**, 2537–2545, https://doi.org/10.1002/2017GL072670.

Min, S.-K., Y.-H. Kim, M.-K. Kim, and C. Park, 2014: Assessing human contribution to the summer 2013 Korean heat wave [in "Explaining Extreme Events of 2013 from a Climate Perspective"]. *Bull. Amer. Meteor. Soc.*, **95** (9), S48–S51, https://doi.org/10.1175/1520-0477-95.9.S1.1.

Miralles, D. G., A. J. Teuling, C. C. van Heerwaarden, and J. V.-G. de Arellano, 2014: Mega-heatwave temperatures due to combined soil desiccation and atmospheric heat accumulation. *Nat. Geosci.*, **7**, 345–349, https://doi.org/10.1038/ngeo2141.

Mohr, K. I., and E. J. Zipser, 1996: Mesoscale convective systems defined by their 85-GHz ice scattering signature: Size and intensity comparison over tropical oceans and continents. *Mon. Wea. Rev.*, **124**, 2417–2437, https://doi.org/10.1175/1520-0493(1996)124<2417:MCSDBT>2.0.CO;2.

Monhart, S., C. Spirig, J. Bhend, K. Bogner, C. Schär, and M. A. Liniger, 2018: Skill of subseasonal forecasts in Europe: Effect of bias correction and downscaling using surface observations. *J. Geophys. Res. Atmos.*, **123**, 7999–8016, https://doi.org/10.1029/2017JD027923.

Mueller, B., and S. I. Seneviratne, 2012: Hot days induced by precipitation deficits at the global scale. *Proc. Natl. Acad. Sci. USA*, **109**, 12 398–12 403, https://doi.org/10.1073/pnas.1204330109.

Muñoz, Á. G., 2020: PyCPT: A Python interface and enhancement for IRI's climate predictability tool. Zenodo, https://doi.org/10.5281/zenodo.3551936.

——, L. Goddard, A. W. Robertson, Y. Kushnir, and W. Baethgen, 2015: Cross-time scale interactions and rainfall extreme events in southeastern South America

for the austral summer. Part I: Potential predictors. *J. Climate*, **28**, 7894–7913, https://doi.org/10.1175/JCLI-D-14-00693.1.

——, ——, S. J. Mason, and A. W. Robertson, 2016: Cross-time scale interactions and rainfall extreme events in southeastern South America for the austral summer. Part II: Predictive skill. *J. Climate*, **29**, 5915–5934, https://doi.org/10.1175/JCLI-D-15-0699.1.

——, and Coauthors, 2019: NextGen: A next-generation system for calibrating, ensembling and verifying regional seasonal and subseasonal forecasts. *2019 Fall Meeting*, San Francisco, CA, Amer. Geophys. Union, Abstract A23U-3024, https://agu.confex.com/agu/fm19/meetingapp.cgi/Paper/581954.

Mylonas, M. P., P. T. Nastos, and I. T. Matsangouras, 2018: PBL parameterization schemes sensitivity analysis on WRF modeling of a tornadic event environment in Skala Lakonia in September 2015. *Atmos. Res.*, **208**, 116–131, https://doi.org/10.1016/j.atmosres.2017.11.023.

Nicholls, N., 1979: A possible method for predicting seasonal tropical cyclone activity in the Australian region. *Mon. Wea. Rev.*, **107**, 1221–1224, https://doi.org/10.1175/1520-0493(1979)107<1221:APMFPS>2.0.CO;2.

NOAA, 2018: Assessing the U.S. climate in July 2018. NOAA, www.ncei.noaa.gov/news/national-climate-201807.

Noer, G., Ø. Saetra, T. Lien, and Y. Gusdal, 2011: A climatological study of polar lows in the Nordic seas. *Quart. J. Roy. Meteor. Soc.*, **137**, 1762–1772, https://doi.org/10.1002/qj.846.

Pan, B., K. Hsu, A. AghaKouchak, S. Sorooshian, and W. Higgins, 2019: Precipitation prediction skill for the West Coast United States: From short to extended range. *J. Climate*, **32**, 161–182, https://doi.org/10.1175/JCLI-D-18-0355.1.

Peng, J.-B., 2014: An investigation of the formation of the heat wave in southern China in summer 2013 and the relevant abnormal subtropical high activities. *Atmos. Ocean. Sci. Lett.*, **7**, 286–290, https://doi.org/10.3878/j.issn.1674-2834.13.0097.

Pepler, A. S., L. B. Díaz, C. Prodhomme, F. J. Doblas-Reyes, and A. Kumar, 2015: The ability of a multi-model seasonal forecasting ensemble to forecast the frequency of warm, cold and wet extremes. *Wea. Climate Extremes*, **9**, 68–77, https://doi.org/10.1016/j.wace.2015.06.005.

Perez-Zanon, N., and Coauthors, 2019: CSTools: Assessing skill of climate forecasts on seasonal-to-decadal timescales, version 2.0.0. R package, http://CRAN.R-project.org/package=CSTools.

Perkins, S., L. Alexander, and J. Nairn, 2012: Increasing frequency, intensity and duration of observed global heatwaves and warm spells. *Geophys. Res. Lett.*, **39**, L20714, https://doi.org/10.1029/2012GL053361.

Pfahl, S., and H. Wernli, 2012: Quantifying the relevance of atmospheric blocking for co-located temperature extremes in the Northern Hemisphere on (sub-)daily time scales. *Geophys. Res. Lett.*, **39**, L12807, https://doi.org/10.1029/2012GL052261.

Pineda, L., J. Changoluisa, and A. Muñoz, 2021: Heavy rainfall in the northern coast of Ecuador in the aftermath of El Niño 2015/2016 and its predictability. *EGU General Assembly*, Online, EGU, EGU21-8559, https://doi.org/10.5194/egusphere-egu21-8559.

Portmann, R., J. J. González-Alemán, M. Sprenger, and H. Wernli, 2020: How an uncertain short-wave perturbation on the North Atlantic wave guide affects the forecast of an intense Mediterranean cyclone (Medicane Zorbas). *Wea. Climate Dyn.*, **1**, 597–615, https://doi.org/10.5194/wcd-2019-1.

Prein, A. F., R. M. Rasmussen, K. Ikeda, C. Liu, M. P. Clark, and G. J. Holland, 2017: The future intensification of hourly precipitation extremes. *Nat. Climate Change*, **7**, 48–52, https://doi.org/10.1038/nclimate3168.

Prior, J., and M. Kendon, 2011: The disruptive snowfalls and very low temperatures of late 2010. *Weather*, **66**, 315–321, https://doi.org/10.1002/wea.874.

Quinting, J. F., and F. Vitart, 2019: Representation of synoptic-scale Rossby wave packets and blocking in the S2S Prediction project database. *Geophys. Res. Lett.*, **46**, 1070–1078, https://doi.org/10.1029/2018GL081381.

Rasmussen, E., 1983: A review of meso-scale disturbances in cold air masses. *Mesoscale Meteorology—Theories, Observations and Models*, Springer, 247–283.

Raymond, C., T. Matthews, and R. M. Horton, 2020: The emergence of heat and humidity too severe for human tolerance. *Sci. Adv.*, **6**, eaaw1838, https://doi.org/10.1126/sciadv.aaw1838.

R Core Team, 2015: R: A language and environment for statistical computing. R Foundation for Statistical Computing, www.R-project.org/.

Risbey, J. S., and Coauthors, 2021: Standard assessments of climate forecast skill can be misleading. *Nat. Commun.*, **12**, 4346, https://doi.org/10.1038/s41467-021-23771-z.

Robertson, A. W., F. Vitart, and S. J. Camargo, 2020: Sub-seasonal to seasonal prediction of weather to climate with application to tropical cyclones. *J. Geophys. Res. Atmos.*, **125**, e2018JD029375, https://doi.org/10.1029/2018JD029375.

Rodney, M., H. Lin, and J. Derome, 2013: Subseasonal prediction of wintertime North American surface air temperature during strong MJO events. *Mon. Wea. Rev.*, **141**, 2897–2909, https://doi.org/10.1175/MWR-D-12-00221.1.

RTE, 2017: Aperçu mensuel sur l'énergie électrique. RTE Tech. Rep., 12 pp., https://assets.rte-france.com/prod/public/2020-06/apercu_energie_elec_2017_01.pdf.

Russo, S., and Coauthors, 2014: Magnitude of extreme heat waves in present climate and their projection in a warming world. *J. Geophys. Res. Atmos.*, **119**, 12 500–12 512, https://doi.org/10.1002/2014JD022098.

Schaller, N., J. Sillmann, J. Anstey, E. M. Fischer, C. M. Grams, and S. Russo, 2018: Influence of blocking on northern European and western Russian heatwaves in large climate model ensembles. *Environ. Res. Lett.*, **13**, 054015, https://doi.org/10.1088/1748-9326/aaba55.

Seneviratne, S. I., T. Corti, E. L. Davin, M. Hirschi, E. B. Jaeger, I. Lehner, B. Orlowsky, and A. J. Teuling, 2010: Investigating soil moisture–climate interactions in a changing climate: A review. *Earth-Sci. Rev.*, **99**, 125–161, https://doi.org/10.1016/j.earscirev.2010.02.004.

Shiogama, H., M. Watanabe, Y. Imada, M. Mori, Y. Kamae, M. Ishii, and M. Kimoto, 2014: Attribution of the June-July 2013 heat wave in the southwestern United States. *SOLA*, **10**, 122–126, https://doi.org/10.2151/sola.2014-025.

Sinclair, V. A., J. W. Mikkola, M. Rantanen, and J. Räisänen, 2019: The summer 2018 heatwave in Finland. *Weather*, **74**, 403–409, https://doi.org/10.1002/wea.3525.

Specq, D., L. Batté, M. Déqué, and C. Ardilouze, 2020: Multimodel forecasting of precipitation at subseasonal timescales over the southwest tropical Pacific. *Earth Space Sci.*, **7**, e2019EA001003, https://doi.org/10.1029/2019EA001003.

Sun, J.-Q., 2012: Possible impact of the summer North Atlantic Oscillation on extreme hot events in China. *Atmos. Ocean. Sci. Lett.*, **5**, 231–234, https://doi.org/10.1080/16742834.2012.11446996.

Sun, L., C. Deser, and R. A. Tomas, 2015: Mechanisms of stratospheric and tropospheric circulation response to projected Arctic Sea ice loss. *J. Climate*, **28**, 7824–7845, https://doi.org/10.1175/JCLI-D-15-0169.1.

Sun, Y., X. Zhang, F. W. Zwiers, L. Song, H. Wan, T. Hu, H. Yin, and G. Ren, 2014: Rapid increase in the risk of extreme summer heat in eastern China. *Nat. Climate Change*, **4**, 1082–1085, https://doi.org/10.1038/nclimate2410.

Thompson, D., M. Baldwin, and J. Wallace, 2002: Stratospheric connection to Northern Hemisphere wintertime weather: Implications for prediction. *J. Climate*, **15**, 1421–1428, https://doi.org/10.1175/1520-0442(2002)015<1421:SCTNHW>2.0.CO;2.

Tian, D., M. Pan, L. Jia, G. Vecchi, and E. F. Wood, 2016: Assessing GFDL high-resolution climate model water and energy budgets from AMIP simulations over Africa. *J. Geophys. Res. Atmos.*, **121**, 8444–8459, https://doi.org/10.1002/2016JD025068.

——, E. F. Wood, and X. Yuan, 2017: CFSv2-based sub-seasonal precipitation and temperature forecast skill over the contiguous United States. *Hydrol. Earth Syst. Sci.*, **21**, 1477–1490, https://doi.org/10.5194/hess-21-1477-2017.

——, M. Pan, and E. F. Wood, 2018: Assessment of a high-resolution climate model for surface water and energy flux simulations over global land: An intercomparison with reanalyses. *J. Hydrometeor.*, **19**, 1115–1129, https://doi.org/10.1175/JHM-D-17-0156.1.

Tippett, M. K., T. DelSole, S. J. Mason, and A. G. Barnston, 2008: Regression-based methods for finding coupled patterns. *J. Climate*, **21**, 4384–4398, https://doi.org/10.1175/2008JCLI2150.1.

Torralba, V., F. J. Doblas-Reyes, D. MacLeod, I. Christel, and M. Davis, 2017: Seasonal climate prediction: A new source of information for the management

of wind energy resources. *J. Appl. Meteor. Climatol.*, **56**, 1231–1247, https://doi.org/10.1175/JAMC-D-16-0204.1.

Ulbrich, U., G. C. Leckebusch, and J. G. Pinto, 2009: Extra-tropical cyclones in the present and future climate: A review. *Theor. Appl. Climatol.*, **96**, 117–131, https://doi.org/10.1007/s00704-008-0083-8.

Vigaud, N., A. W. Robertson, and M. K. Tippett, 2017: Multimodel ensembling of subseasonal precipitation forecasts over North America. *Mon. Wea. Rev.*, **145**, 3913–3928, https://doi.org/10.1175/MWR-D-17-0092.1.

Vitart, F., 2014: Evolution of ECMWF sub-seasonal forecast skill scores. *Quart. J. Roy. Meteor. Soc.*, **140**, 1889–1899, https://doi.org/10.1002/qj.2256.

——, 2017: Madden-Julian oscillation prediction and teleconnections in the S2S. *Quart. J. Roy. Meteor. Soc.*, **143**, 2210–2220, https://doi.org/10.1002/qj.3079.

——, and F. Molteni, 2010: Simulation of the Madden–Julian oscillation and its teleconnections in the ECMWF Forecast System. *Quart. J. Roy. Meteor. Soc.*, **136**, 842–855, https://doi.org/10.1002/qj.623.

——, and A. W. Robertson, 2018: The Sub-Seasonal to Seasonal Prediction project (S2S) and the prediction of extreme events. *npj Climate Atmos. Sci.*, **1**, 3, https://doi.org/10.1038/s41612-018-0013-0.

——, J. L. Anderson, and W. F. Stern, 1997: Simulation of interannual variability of tropical storm frequency in an ensemble of GCM integrations. *J. Climate*, **10**, 745–760, https://doi.org/10.1175/1520-0442(1997)010<0745:SOIVOT>2.0.CO;2.

——, D. Anderson, and T. Stockdale, 2003: Seasonal forecasting of tropical cyclone landfall over Mozambique. *J. Climate*, **16**, 3932–3945, https://doi.org/10.1175/1520-0442(2003)016<3932:SFOTCL>2.0.CO;2.

——, and Coauthors, 2008: The new VarEPS-monthly forecasting system: A first step towards seamless prediction. *Quart. J. Roy. Meteor. Soc.*, **134**, 1789–1799, https://doi.org/10.1002/qj.322.

——, A. Leroy, and M. C. Wheeler, 2010: A comparison of dynamical and statistical predictions of weekly tropical cyclone activity in the Southern Hemisphere. *Mon. Wea. Rev.*, **138**, 3671–3682, https://doi.org/10.1175/2010MWR3343.1.

——, and Coauthors, 2017: The Subseasonal to Seasonal (S2S) Prediction project database. *Bull. Amer. Meteor. Soc.*, **98**, 163–173, https://doi.org/10.1175/BAMS-D-16-0017.1.

——, and Coauthors, 2019: Sub-seasonal to seasonal prediction of weather extremes. *Sub-Seasonal to Seasonal Prediction*, A. W. Robertson and F. Vitart, Eds., Elsevier, 365–386.

Wang, J., Z. Yan, X.-W. Quan, and J. Feng, 2017: Urban warming in the 2013 summer heat wave in eastern China. *Climate Dyn.*, **48**, 3015–3033, https://doi.org/10.1007/s00382-016-3248-7.

Watanabe, M., H. Shiogama, Y. Imada, M. Mori, M. Ishii, and M. Kimoto, 2013: Event attribution of the August 2010 Russian heat wave. *SOLA*, **9**, 65–68, https://doi.org/10.2151/sola.2013-015.

Wernli, H., M. Paulat, M. Hagen, and C. Frei, 2008: SAL—A novel quality measure for the verification of quantitative precipitation forecasts. *Mon. Wea. Rev.*, **136**, 4470–4487, https://doi.org/10.1175/2008MWR2415.1.

Westra, S., L. V. Alexander, and F. W. Zwiers, 2013: Global increasing trends in annual maximum daily precipitation. *J. Climate*, **26**, 3904–3918, https://doi.org/10.1175/JCLI-D-12-00502.1.

Wheeler, M. C., and H. H. Hendon, 2004: An all-season real-time multivariate MJO index: Development of an index for monitoring and prediction. *Mon. Wea. Rev.*, **132**, 1917–1932, https://doi.org/10.1175/1520-0493(2004)132<1917:AARMMI>2.0.CO;2.

White, C. J., and Coauthors, 2017: Potential applications of subseasonal-to-seasonal (S2S) predictions. *Meteor. Appl.*, **24**, 315–325, https://doi.org/10.1002/met.1654.

——, and Coauthors, 2022: Advances in the application and utility of subseasonal-to-seasonal predictions. *Bull. Amer. Meteor. Soc.*, https://doi.org/10.1175/BAMS-D-20-0224.1, in press.

Wilks, D. S., 2019: *Statistical Methods in the Atmospheric Sciences.* 4th ed. Elsevier/Academic Press, 840 pp.

Wirth, V., M. Riemer, E. K. M. Chang, and O. Martius, 2018: Rossby wave packets on the midlatitude waveguide—A review. *Mon. Wea. Rev.*, **146**, 1965–2001, https://doi.org/10.1175/MWR-D-16-0483.1.

WMO, 2020: Guidance on operational practices for objective seasonal forecasting. WMO Tech. Rep. WMO-1246, 106 pp., https://library.wmo.int/index.php?lvl=notice_display&id=21741#.YnPlm9rMKUk.

WorldBank, 2018: Concatenated volcanic hazards: Fuego volcano crisis. WorldBank Rep., 102 pp., https://documents1.worldbank.org/curated/zh/360901560919670273/pdf/Concatenated-Volcanic-Hazards-Fuego-Volcano-Crisis.pdf.

Wu, B., T. Zhou, and T. Li, 2016: Impacts of the Pacific–Japan and circumglobal teleconnection patterns on the interdecadal variability of the East Asian summer monsoon. *J. Climate*, **29**, 3253–3271, https://doi.org/10.1175/JCLI-D-15-0105.1.

Wulff, C. O., and D. I. V. Domeisen, 2019: Higher subseasonal predictability of extreme hot European summer temperatures as compared to average summers. *Geophys. Res. Lett.*, **46**, 11 520–11 529, https://doi.org/10.1029/2019GL084314.

——, R. J. Greatbatch, D. I. V. Domeisen, G. Gollan, and F. Hansen, 2017: Tropical forcing of the summer East Atlantic pattern. *Geophys. Res. Lett.*, **44**, 1083–1088, https://doi.org/10.1002/2017GL075493.

Yang, J., and Coauthors, 2019: Heatwave and mortality in 31 major Chinese cities: Definition, vulnerability and implications. *Sci. Total Environ.*, **649**, 695–702, https://doi.org/10.1016/j.scitotenv.2018.08.332.

Yasui, S., and M. Watanabe, 2010: Forcing processes of the summertime circumglobal teleconnection pattern in a dry AGCM. *J. Climate*, **23**, 2093–2114, https://doi.org/10.1175/2009JCLI3323.1.

Yeo, S.-R., S.-W. Yeh, and W.-S. Lee, 2019: Two types of heat wave in Korea associated with atmospheric circulation pattern. *J. Geophys. Res. Atmos.*, **124**, 7498–7511, https://doi.org/10.1029/2018JD030170.

Yiou, P., and Coauthors, 2019: Analyses of the northern European summer heatwave of 2018 [in "Explaining Extreme Events of 2018 from a Climate Perspective"]. *Bull. Amer. Meteor. Soc.*, **101** (1), S35–S40, https://doi.org/10.1175/BAMS-D-19-0170.1.

Zhang, W., and T. Zhou, 2019: Significant increases in extreme precipitation and the associations with global warming over the global land monsoon regions. *J. Climate*, **32**, 8465–8488, https://doi.org/10.1175/JCLI-D-18-0662.1.

Zhang, X., H. Wan, F. W. Zwiers, G. C. Hegerl, and S.-K. Min, 2013: Attributing intensification of precipitation extremes to human influence. *Geophys. Res. Lett.*, **40**, 5252–5257, https://doi.org/10.1002/grl.51010.

Zscheischler, J., and Coauthors, 2020: A typology of compound weather and climate events. *Nat. Rev. Earth Environ.*, **1**, 333–347, https://doi.org/10.1038/s43017-020-0060-z.